J|A|C|S
ARTICLES
Published on Web 04/17/2002

Mixed-Metal Cluster Chemistry. 19. Crystallographic, Spectroscopic, Electrochemical, Spectroelectrochemical, and Theoretical Studies of Systematically Varied Tetrahedral Group 6−Iridium Clusters

Nigel T. Lucas,[†] Jonathan P. Blitz,[†,||] Simon Petrie,[†] Robert Stranger,[†] Mark G. Humphrey,*[,†] Graham A. Heath,[‡] and Vincent Otieno-Alego[§]

Contribution from the Department of Chemistry, Australian National University, Canberra ACT 0200, Australia, Research School of Chemistry, Australian National University, Canberra ACT 0200, Australia, and Division of Science and Design, University of Canberra, Canberra ACT 2601, Australia

Received October 24, 2001

Abstract: A systematically varied series of tetrahedral clusters involving ligand and core metal variation has been examined using crystallography, Raman spectroscopy, cyclic voltammetry, UV−vis−NIR and IR spectroelectrochemistry, and approximate density functional theory, to assess cluster rearrangement to accommodate steric crowding, the utility of metal−metal stretching vibrations in mixed-metal cluster characterization, and the possibility of tuning cluster electronic structure by systematic modification of composition, and to identify cluster species resultant upon electrochemical oxidation or reduction. The 60-electron tetrahedral clusters $MIr_3(CO)_{11-x}(PMe_3)_x(\eta^5\text{-Cp})$ [M = Mo, $x = 0$, Cp = C_5H_4Me (**5**), C_5HMe_4 (**6**), C_5Me_5 (**7**); M = W, Cp = C_5H_4Me, $x = 1$ (**13**), $x = 2$ (**14**)] and $M_2Ir_2(CO)_{10-x}(PMe_3)_x(\eta^5\text{-Cp})$ [M = Mo, $x = 0$, Cp = C_5H_4Me (**8**), C_5HMe_4 (**9**), C_5Me_5 (**10**); M = W, Cp = C_5H_4Me, $x = 1$ (**15**), $x = 2$ (**16**)] have been prepared. Structural studies of **7**, **10**, and **13** have been undertaken; these clusters are among the most sterically encumbered, compensating by core bond lengthening and unsymmetrical carbonyl dispositions (semi-bridging, semi-face-capping). Raman spectra for **5**, **8**, $WIr_3(CO)_{11}(\eta^5\text{-}C_5H_4Me)$ (**11**), and $W_2Ir_2(CO)_{10}(\eta^5\text{-}C_5H_4Me)_2$ (**12**), together with the spectrum of $Ir_4(CO)_{12}$, have been obtained, the first Raman spectra for mixed-metal clusters. Minimal mode-mixing permits correlation between A_1 frequencies and cluster core bond strength, frequencies for the A_1 breathing mode decreasing on progressive group 6 metal incorporation, and consistent with the trend in metal−metal distances [Ir−Ir < M−Ir < M−M]. Cyclic voltammetric scans for **5**−**15**, $MoIr_3(CO)_{11}(\eta^5\text{-}C_5H_5)$ (**1**), and $Mo_2Ir_2(CO)_{10}(\eta^5\text{-}C_5H_5)_2$ (**3**) have been collected. The [MIr_3] clusters show irreversible one-electron reduction at potentials which become negative on cyclopentadienyl alkyl introduction, replacement of molybdenum by tungsten, and replacement of carbonyl by phosphine. These clusters show two irreversible one-electron oxidation processes, the easier of which tracks with the above structural modifications; a third irreversible oxidation process is accessible for the bis-phosphine cluster **14**. The [M_2Ir_2] clusters show irreversible two-electron reduction processes; the tungsten-containing clusters and phosphine-containing clusters are again more difficult to reduce than their molybdenum-containing or carbonyl-containing analogues. These clusters show two one-electron oxidation processes, the easier of which is reversible/quasi-reversible, and the more difficult of which is irreversible; the former occur at potentials which increase on cyclopentadienyl alkyl removal, replacement of tungsten by molybdenum, and replacement of phosphine by carbonyl. The reversible one-electron oxidation of **12** has been probed by UV−vis−NIR and IR spectroelectrochemistry. The former reveals that $\mathbf{12}^+$ has a low-energy band at 8000 cm^{-1}, a spectrally transparent region for **12**, and the latter reveals that $\mathbf{12}^+$ exists in solution with an all-terminal carbonyl geometry, in contrast to **12** for which an isomer with bridging carbonyls is apparent in solution. Approximate density functional calculations (including ZORA scalar relativistic corrections) have been undertaken on the various charge states of $W_2Ir_2(CO)_{10}(\eta^5\text{-}C_5H_5)_2$ (**4**). The calculations suggest that two-electron reduction is accompanied by W−W cleavage, whereas one-electron oxidation proceeds with retention of the tetrahedral core geometry. The calculations also suggest that the low-energy NIR band of $\mathbf{12}^+$ arises from a σ(W−W) → σ^*(W−W) transition.

Introduction

Transition metal carbonyl cluster compounds have attracted significant interest for a variety of reasons including, inter alia, the transition from molecular to bulk metallic properties which should ensue upon increasing cluster size,[1−3] as models for metal surfaces in chemisorption and catalysis,[4−12] and as precursors for metal particles active in heterogeneous catalysis.[6,7,9,10,12] The

* Corresponding author. Phone: +61 2 6125 2927. Fax: +61 2 6125 0760. E-mail: Mark.Humphrey@anu.edu.au.
[†] Department of Chemistry.
[‡] Research School of Chemistry.
[§] Division of Science and Design.
[||] On leave from Eastern Illinois University.

(1) Schmid, G. *Clusters and Colloids: From Theory to Applications*; VCH: Weinheim, 1994.
(2) de Jongh, L. J. *Physics and Chemistry of Metal Cluster Compounds*; Kluwer: Dordrecht, 1994.
(3) Cifuentes, M. P.; Humphrey, M. G.; McGrady, J. E.; Smith, P. J.; Stranger, R.; Murray, K. S.; Moubaraki, B. *J. Am. Chem. Soc.* **1997**, *119*, 2647.

electronic structure of clusters has been examined from several perspectives to facilitate detailed understanding. Studies of cluster electrochemistry,[13−19] carried out frequently in concert with electronic structure calculations,[20−39] have afforded information about the highest occupied molecular orbitals (HOMOs) and lowest unoccupied molecular orbitals (LUMOs). Calculations using density functional theory have been promulgated to enhance understanding of spectroscopic properties, charge distributions, and reactivities.[3,37−52] Cluster electrochemistry, in combination with IR and UV−visible spectroelectrochemistry and frequently EPR, has afforded insight into the electronic and molecular structure of clusters in varying oxidation states.[28,53−69]

The great majority of studies probing electronic structure of transition metal carbonyl clusters have focused on homometallic clusters. Mixed-metal clusters (particularly those with disparate metals) are of interest for a number of reasons: for example, cooperative effects between adjacent metal centers could be enhanced by the presence of a polar metal−metal bond, sufficiently different metals should "select" for particular types of reagents,[70] bimetallic clusters may be precursors for catalytically active species with well-defined metal:metal stoichiometry, and the differing metals in such clusters provide effective labels for ligand fluxionality studies.[71] While efficient synthetic routes to "very mixed"-metal clusters (those containing metals which differ by three or more *d*-block groups)[72] have been documented, reactivity studies are significantly less extensive, and reports of physical properties comparatively scarce. Specifically, the possibility of controlling and tuning the electronic properties of clusters by sequential introduction of heterometals is of particular interest, but is thus far little-investigated. We present herein a detailed electrochemical, spectroelectrochemical, and theoretical study of the group 6−iridium clusters $M_nIr_{4-n}(CO)_{12-n}Cp_n$

(4) Muetterties, E. L.; Rhodin, T. N.; Band, E.; Brucker, C. F.; Pretzer, W. R. *Chem. Rev.* **1979**, *79*, 91.
(5) Evans, J. *Chem. Soc. Rev.* **1981**, *10*, 159.
(6) Moskovits, M. In *Metal Clusters*; Moskovits, M., Ed.; John Wiley: New York, 1986; p 1.
(7) Gates, B. C. In *Metal Clusters in Catalysis*; Gates, B. C., Guczi, L., Knözinger, H., Eds.; Elsevier: Amsterdam, 1986.
(8) Puddephatt, R. J.; Manojlovic-Muir, L.; Muir, K. W. *Polyhedron* **1990**, *9*, 2767.
(9) Adams, R. D.; Cotton, F. A. *Catalysis by di- and polynuclear metal cluster complexes*; Wiley-VCH: New York, 1998.
(10) Braunstein, P.; Oro, L. A.; Raithby, P. R. In *Metal Clusters in Chemistry*; Braunstein, P., Oro, L. A., Raithby, P. R., Eds.; Wiley-VCH: Weinheim, Germany, 1999; Vol. 2.
(11) Overett, M. J.; Hill, R. O.; Moss, J. R. *Coord. Chem. Rev.* **2000**, *206−207*, 581.
(12) Gates, B. C. *J. Mol. Catal. A: Chem.* **2000**, *163*, 55.
(13) Lemoine, P. *Coord. Chem. Rev.* **1982**, *47*, 55.
(14) Geiger, W. E.; Connelly, N. G. *Adv. Organomet. Chem.* **1985**, *24*, 87.
(15) Lemoine, P. *Coord. Chem. Rev.* **1988**, *83*, 169.
(16) Drake, S. R. *Polyhedron* **1990**, *9*, 455.
(17) Zanello, P. In *Structure and Bonding*; Clarke, M. J., Goodenough, J. B., Jørgensen, C. K., Neilands, J. B., Reinen, D., Weiss, R., Eds.; Springer: Berlin, 1992; Vol. 79, p 101.
(18) Zanello, P. In *Stereochemistry of Organometallic and Inorganic Compounds*; Zanello, P., Ed.; Elsevier: Amsterdam, 1994; Vol. 5, p 181.
(19) Zanello, P.; de Biani, F. F. In *Metal Clusters in Chemistry*; Braunstein, P., Oro, L. A., Raithby, P. R., Eds.; Wiley-VCH: Weinheim, Germany, 1999; Vol. 2, p 1104.
(20) Holland, G. F.; Ellis, D. E.; Trogler, W. C. *J. Am. Chem. Soc.* **1986**, *108*, 1884.
(21) Holland, G. F.; Ellis, D. E.; Tyler, D. R.; Gray, H. B.; Trogler, W. C. *J. Am. Chem. Soc.* **1987**, *109*, 4276.
(22) Albright, T. A.; Kang, S.-K.; Arif, A. M.; Bard, A. J.; Jones, R. A.; Leland, J. K.; Schwab, S. T. *Inorg. Chem.* **1988**, *27*, 1246.
(23) Leigh, J. S.; Whitmire, K. H.; Yee, K. A.; Albright, T. A. *J. Am. Chem. Soc.* **1989**, *111*, 2726.
(24) Osella, D.; Arman, G.; Gobetto, R.; Laschi, F.; Zanello, P.; Ayrton, S.; Goodfellow, V.; Housecroft, C. E.; Owen, S. M. *Organometallics* **1989**, *8*, 2689.
(25) Albano, V. G.; Demartin, F.; Iapalucci, M. C.; Laschi, F.; Longoni, G.; Sironi, A.; Zanello, P. *J. Chem. Soc., Dalton Trans.* **1991**, 739.
(26) Albright, T. A.; Yee, K.-A.; Saillard, J.-Y.; Kahlal, S.; Halet, J.-F.; Leigh, J. S.; Whitmire, K. H. *Inorg. Chem.* **1991**, *30*, 1179.
(27) Osella, D.; Ravera, M.; Nervi, C.; Housecroft, C. E.; Raithby, P. R.; Zanello, P.; Laschi, F. *Organometallics* **1991**, *10*, 3253.
(28) Koide, Y.; Bautista, M. T.; White, P. S.; Schauer, C. K. *Inorg. Chem.* **1992**, *31*, 3690.
(29) North, T. E.; Thoden, J. B.; Spencer, B.; Bjarnason, A.; Dahl, L. F. *Organometallics* **1992**, *11*, 4326.
(30) Lugan, N.; Fabre, P.-L.; de Montauzon, D.; Lavigne, G.; Bonnet, J.-J.; Saillard, J.-Y.; Halet, J.-F. *Inorg. Chem.* **1993**, *32*, 1363.
(31) Shen, H.; Williams, T. J.; Bott, S. G.; Richmond, M. G. *J. Organomet. Chem.* **1995**, *505*, 1.
(32) Shen, H.; Bott, S. G.; Richmond, M. G. *Inorg. Chim. Acta* **1996**, *241*, 71.
(33) Xia, C.-G.; Yang, K.; Bott, S. G.; Richmond, M. G. *Organometallics* **1996**, *15*, 4480.
(34) Collins, B. E.; Koide, Y.; Schauer, C. K.; White, P. S. *Inorg. Chem.* **1997**, *36*, 6172.
(35) Gauthron, I.; Mugnier, Y.; Hierso, K.; Harvey, P. D. *Can. J. Chem.* **1997**, *75*, 1182.
(36) Yao, H.; McCargar, R. D.; Allendoerfer, R. D.; Keister, J. B.; Low, A. A. *J. Organomet. Chem.* **1998**, *568*, 63.
(37) Brunner, H.; Lucas, D.; Monzon, T.; Mugnier, Y.; Nuber, B.; Stubenhofer, B.; Stückl, A. C.; Wachter, J.; Wanninger, R.; Zabel, M. *Chem. Eur. J.* **2000**, *6*, 493.
(38) Ho, E. N.-M.; Lin, Z.; Wong, W.-T. *Eur. J. Inorg. Chem.* **2001**, 1321.
(39) Ho, E. N.-M.; Lin, Z.; Wong, W.-T. *Chem. Eur. J.* **2001**, *7*, 258.
(40) Manning, M. C.; Trogler, W. C. *Coord. Chem. Rev.* **1981**, *38*, 89.
(41) Trogler, W. C. *Acc. Chem. Res.* **1990**, *23*, 239.
(42) Albert, K.; Neyman, K. M.; Pacchioni, G.; Rösch, N. *Inorg. Chem.* **1996**, *35*, 7370.
(43) Liddell, M. J. *J. Organomet. Chem.* **1998**, *565*, 271.
(44) Zouchoune, B.; Ogliaro, F.; Halet, J.-F.; Saillard, J.-Y.; Eveland, J. R.; Whitmire, K. H. *Inorg. Chem.* **1998**, *37*, 865.
(45) Beringhelli, T.; D'Alfonso, G.; Panigati, M.; Porta, F.; Mercandelli, P.; Moret, M.; Sironi, A. *J. Am. Chem. Soc.* **1999**, *121*, 2307.
(46) Bruce, M. I.; Humphrey, P. A.; Skelton, B. W.; White, A. H.; Costuas, K.; Halet, J.-F. *J. Chem. Soc., Dalton Trans.* **1999**, 479.
(47) Stener, M.; Albert, K.; Rösch, N. *Inorg. Chim. Acta* **1999**, *286*, 30.
(48) Abarca, A.; Galakhov, M.; Gómez-Sal, P.; Martín, A.; Mena, M.; Poblet, J.-M.; Santamaria, C.; Sarasa, J. P. *Angew. Chem., Int. Ed.* **2000**, *39*, 534.
(49) Bruce, M. I.; Low, P. J.; Zaitseva, N. N.; Kahlal, S.; Halet, J.-F.; Skelton, B. W.; White, A. H. *J. Chem. Soc., Dalton Trans.* **2000**, 2939.
(50) Wang, W.; Low, P. J.; Carty, A. J.; Sappa, E.; Gervasio, G.; Mealli, C.; Ienco, A.; Perez-Carreño, E. *Inorg. Chem.* **2000**, *39*, 998.
(51) Adams, C. J.; Bruce, M. I.; Halet, J.-F.; Kahlal, S.; Skelton, B. W.; White, A. H. *J. Chem. Soc., Dalton Trans.* **2001**, 414.
(52) Saillard, J.-Y.; Kahlal, S.; Ferrand, V.; Stoeckli-Evans, H.; Süss-Fink, G. *J. Organomet. Chem.* **2001**, *620*, 119.
(53) Arce, A. J.; Bates, P. A.; Best, S. P.; Clark, R. J. H.; Deeming, A. J.; Hursthouse, M. B.; McQueen, R. C. S.; Powell, N. I. *J. Chem. Soc., Chem. Commun.* **1988**, 478.
(54) Fish, J. R.; Malinski, T.; Mayr, A. J.; Pannell, K. H. *Inorg. Chim. Acta* **1988**, *150*, 249.
(55) Lewis, G. J.; Roth, J. D.; Montag, R. A.; Safford, L. K.; Gao, X.; Chang, S.-C.; Dahl, L. F.; Weaver, M. J. *J. Am. Chem. Soc.* **1990**, *112*, 2831.
(56) Best, S. P.; Clark, R. J. H.; Deeming, A. J.; McQueen, R. C. S.; Powell, N. I.; Acuña, C.; Arce, A. J.; De Sanctis, Y. *J. Chem. Soc., Dalton Trans.* **1991**, 1111.
(57) Roth, J. D.; Lewis, G. J.; Safford, L. K.; Jiang, X.; Dahl, L. F.; Weaver, M. J. *J. Am. Chem. Soc.* **1992**, *114*, 6159.
(58) Washington, J.; Kubiak, C. P. *Can. J. Chem.* **1996**, *74*, 2503.
(59) van den Berg, W.; Boot, L.; Joosen, H.; van der Linden, J. G. M.; Bosman, W. P.; Smits, J. M. M.; de Gelder, R.; Beurskens, P. T.; Heck, J.; Gal, A. W. *Inorg. Chem.* **1997**, *36*, 1821.
(60) Cifuentes, M. P.; Humphrey, M. G.; Heath, G. A. *Inorg. Chim. Acta* **1997**, *259*, 273.
(61) Geiger, W. E.; Shaw, M. J.; Wünsch, M.; Barnes, C. E.; Foersterling, F. H. *J. Am. Chem. Soc.* **1997**, *119*, 2804.
(62) Wittrig, R. E.; Ferrence, G. M.; Washington, J.; Kubiak, C. P. *Inorg. Chim. Acta* **1998**, *270*, 111.
(63) Nijhoff, J.; Bakker, M. J.; Hartl, F.; Freeman, G.; Ingham, S. L.; Johnson, B. F. G. *J. Chem. Soc., Dalton Trans.* **1998**, 2625.
(64) Brooksby, P. A.; Duffy, N. W.; McQuillan, A. J.; Robinson, B. H.; Simpson, J. *J. Chem. Soc., Dalton Trans.* **1998**, 2855.
(65) Clark, R. J. H.; Dyson, P. J.; Humphrey, D. G.; Johnson, B. F. G. *Polyhedron* **1998**, *17*, 2985.
(66) Nijhoff, J.; Hartl, F.; van Outersterp, J. W. M.; Stufkens, D. J.; Calhorda, M. J.; Veiros, L. F. *J. Organomet. Chem.* **1999**, *573*, 121.
(67) Robben, M. P.; Rieger, P. H.; Geiger, W. E. *J. Am. Chem. Soc.* **1999**, *121*, 367.
(68) Rosenberg, E.; Abedin, M. J.; Rokhsana, D.; Osella, D.; Milone, L.; Nervi, C.; Fiedler, J. *Inorg. Chim. Acta* **2000**, *300−302*, 769.
(69) Wadepohl, H.; Gebert, S.; Pritzkow, H.; Osella, D.; Nervi, C.; Fiedler, J. *Eur. J. Inorg. Chem.* **2000**, 1833.
(70) Lee, J.; Humphrey, M. G.; Hockless, D. C. R.; Skelton, B. W.; White, A. H. *Organometallics* **1993**, *12*, 3468.
(71) Waterman, S. M.; Humphrey, M. G.; Tolhurst, V.-A.; Bruce, M. I.; Low, P. J.; Hockless, D. C. R. *Organometallics* **1998**, *17*, 5789.
(72) Waterman, S. M.; Lucas, N. T.; Humphrey, M. G. In *Adv. Organomet. Chem.*; Hill, A., West, R., Eds.; Academic Press: New York, 2000; Vol. 46, p 47.

Scheme 1. Syntheses of $MoIr_3(CO)_{11}(\eta^5\text{-}C_5H_{5-n}Me_n)$, $n = 1$ (**5**), 4 (**6**), and 5 (**7**)

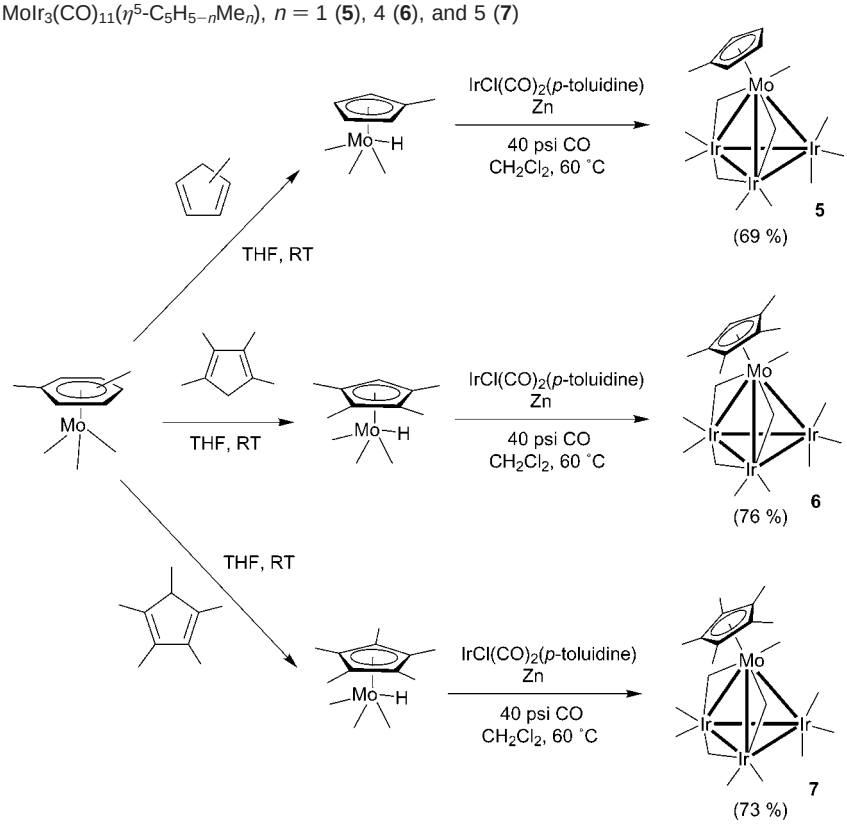

(M = Mo, W; $n = 1$, 2; Cp = C_5H_5, C_5H_4Me, C_5HMe_4, C_5Me_5; not all combinations) and some of their phosphine substitution products. These clusters are derived from the extensively studied[73] tetrahedral cluster $Ir_4(CO)_{12}$ by conceptual replacement of $Ir(CO)_3$ vertices by isolobal $M(CO)_2Cp$ units. This systematically varied series provides the opportunity to assess trends in oxidation/reduction potentials by cyclic voltammetry, and thereby test ligand-additivity[74] ideas and previously unexplored metal-additivity possibilities; this will therefore afford a glimpse of the prospects of controlling cluster electronic properties by core metal and peripheral ligand variation. Increasing the steric bulk of ligands in *closo* polyhedral clusters may potentially result in disruption of metal−metal connectivity or drastic changes in ligand coordination modes. For the present series, structural studies of the pentamethylcyclopentadienyl-containing clusters afford the opportunity to assess this for some of the most sterically crowded tetranuclear clusters thus far. Raman spectroscopy is particularly useful for examining metal−metal bonding, and has been applied to a range of transition metal carbonyl clusters.[75−83] Thus far, however, all studies have involved examining homometallic clusters, one reason being the increased complication in Raman spectra resulting from the decrease in symmetry on proceeding from homometallic cluster to isostructural heterometallic cluster. The first Raman spectroscopic data for mixed-metal clusters are reported herein, and have been assigned utilizing the systematic variation inherent in this system. Although electrochemically induced oxidation/reduction processes in many clusters have been reported, few reports detail structural assignment of the oxidized/reduced species. The reduction in molecular symmetry in proceeding from homometallic to heterometallic cluster may facilitate such identification. We also report herein the first combined IR- and UV−vis spectroelectrochemical study of oxidation and reduction processes in very-mixed-metal clusters, rationalized with the aid of density functional theory (DFT) calculations, permitting structural suggestions for the oxidized and reduced species, and spectral assignment of the important electronic transitions.

Results and Discussion

Syntheses and Characterization of $MoIr_3(CO)_{11}(\eta^5\text{-}C_5H_{5-n}Me_n)$ and $Mo_2Ir_2(CO)_{10}(\eta^5\text{-}C_5H_{5-n}Me_n)_2$ Clusters (n = 1, 4, 5). The air-sensitive hydrides $MoH(CO)_3(\eta^5\text{-}C_5H_{5-n}Me_n)$ ($n = 1$, 4, 5) were prepared by the facile reaction of the commercially available methyl-substituted cyclopentadienes $C_5H_{6-n}Me_n$ with $Mo(CO)_3(\eta^6\text{-xylene})$ at room temperature (Scheme 1), a modification on a literature procedure.[84] An excess of the crude hydride $MoH(CO)_3(\eta^5\text{-}C_5H_{5-n}Me_n)$ was combined with $IrCl(CO)_2$(*p*-toluidine) in the presence of zinc (as reducing agent), and the mixture heated under a carbon monoxide atmosphere to afford $MoIr_3(CO)_{11}(\eta^5\text{-}C_5H_4Me)$ (69%) (**5**), $MoIr_3(CO)_{11}(\eta^5\text{-}C_5HMe_4)$ (76%) (**6**), and $MoIr_3(CO)_{11}(\eta^5\text{-}$

(73) Barnes, C. In *Comprehensive Organometallic Chemistry II*; Abel, E. W., Stone, F. G. A., Wilkinson, G., Eds.; Pergamon: New York, 1996; Vol. 8, p 490.
(74) Lever, A. B. P. *Inorg. Chem.* **1990**, *29*, 1271.
(75) Quicksall, C. O.; Spiro, T. G. *Inorg. Chem.* **1968**, *7*, 2365.
(76) Quicksall, C. O.; Spiro, T. G. *Inorg. Chem.* **1969**, *8*, 2011.
(77) Quicksall, C. O.; Spiro, T. G. *Inorg. Chem.* **1970**, *9*, 1045.
(78) Deeba, M.; Streusand, B. J.; Schrader, G. L.; Gates, B. C. *J. Catal.* **1981**, *69*, 218.
(79) Delley, B.; Manning, M. C.; Ellis, D. E.; Berkowitz, J.; Trogler, W. C. *Inorg. Chem.* **1982**, *21*, 2247.
(80) Diana, E.; Gervasio, G.; Rossetti, R.; Valdemarin, F.; Bor, G.; Stanghellini, P. L. *Inorg. Chem.* **1991**, *30*, 294.
(81) Harvey, P. D.; Shafiq, F.; Eisenberg, R. *Inorg. Chem.* **1994**, *33*, 3424.
(82) Gervasio, G.; Kettle, S. F. A.; Musso, F.; Rossetti, R.; Stanghellini, P. L. *Inorg. Chem.* **1995**, *34*, 298.
(83) Parker, S. F.; Dallin, P. H.; Keiller, B. T.; Anson, C. E.; Jayasooriya, U. A. *Phys. Chem. Chem. Phys.* **1999**, *1*, 2589.
(84) Nolan, S. P.; Hoff, C. D. *Organomet. Synth.* **1988**, *4*, 58.

Scheme 2. Syntheses of $Mo_2Ir_2(CO)_{10}(\eta^5\text{-}C_5H_{5-n}Me_n)_2$, $n = 1$ (**8**), 4 (**9**), and 5 (**10**)

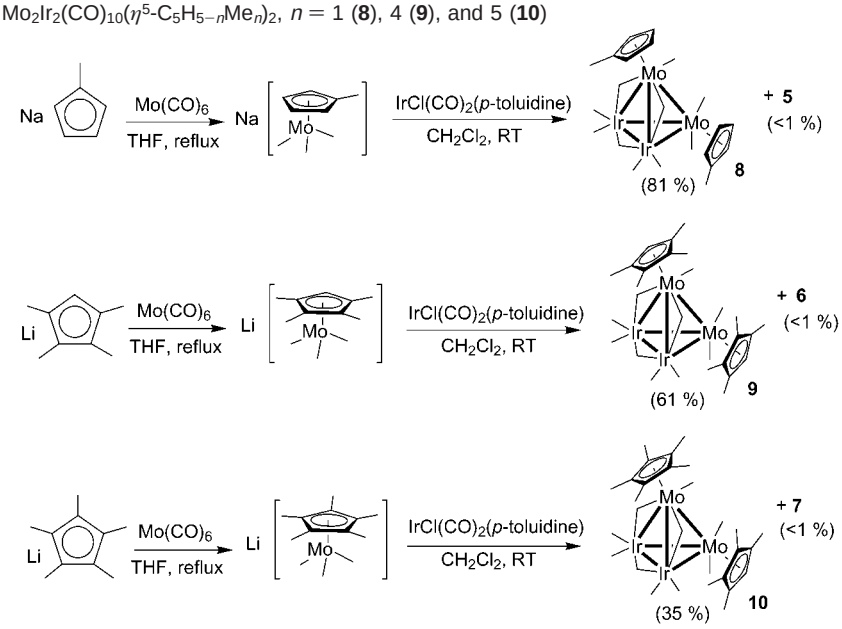

C_5Me_5) (73%) (**7**), respectively (Scheme 1). The cyclopentadienyl analogue of these clusters, $MoIr_3(CO)_{11}(\eta^5\text{-}C_5H_5)$ (**1**), has been prepared in 60% yield by a similar procedure.[85] Workup is simplified by the addition of a small quantity of CCl_4 to the reaction mixture after reaction, but before exposure to air. This converts unreacted $MoH(CO)_3(\eta^5\text{-}C_5H_{5-n}Me_n)$ to $MoCl(CO)_3(\eta^5\text{-}C_5H_{5-n}Me_n)$ before oxidation of the former occurs to afford the $\{Mo(CO)_3(\eta^5\text{-}C_5H_{5-n}Me_n)\}_2$ dimer, as the dimer was found to be difficult to chromatographically separate from the products.

The anions $[Mo(CO)_3(\eta^5\text{-}C_5H_{5-n}Me_n)]^-$ ($n = 1, 4, 5$) were generated by reaction of $Mo(CO)_6$ with the corresponding sodium or lithium cyclopentadienide salts, the latter prepared in situ from commercially available methyl-substituted cyclopentadienes $C_5H_{6-n}Me_n$.[86] Reaction of $IrCl(CO)_2$(*p*-toluidine) with an excess of the anion $[Mo(CO)_3(\eta\text{-}C_5H_{5-n}Me_n)]^-$ afforded $Mo_2Ir_2(CO)_{10}(\eta^5\text{-}C_5H_4Me)_2$ (81%) (**8**), $Mo_2Ir_2(CO)_{10}(\eta^5\text{-}C_5HMe_4)_2$ (61%) (**9**), and $Mo_2Ir_2(CO)_{10}(\eta^5\text{-}C_5Me_5)_2$ (35%) (**10**), respectively (Scheme 2), with the respective molybdenum−triiridium clusters **5**−**7** being isolated as minor products. The synthetic methodology used to prepare **8**−**10** is based on the procedure described for the preparation of the related cyclopentadienyl analogue $Mo_2Ir_2(CO)_{10}(\eta^5\text{-}C_5H_5)_2$ (**3**) in 78% yield,[87] and tungsten−iridium analogues $W_2Ir_2(CO)_{10}(\eta^5\text{-}C_5H_5)_2$[88] (**4**) and $W_2Ir_2(CO)_{10}(\eta^5\text{-}C_5H_4Me)_2$[89] in 81−85% yield. One modification to the literature method was to convert the excess anion to the related hydride $MoH(CO)_3(\eta^5\text{-}C_5H_{5-n}Me_n)$ by addition of acetic acid, which was then converted to $MoCl(CO)_3(\eta^5\text{-}C_5H_{5-n}Me_n)$ by addition of CCl_4 as described above.

The products **5**−**10** have all been characterized by a combination of IR, ^{1}H NMR, and UV−vis spectroscopies, SI mass spectrometry, and satisfactory microanalysis. The solution IR spectra in cyclohexane indicate the presence of terminal and bridging carbonyl ligands, in contrast to the tungsten-containing analogues $WIr_3(CO)_{11}(\eta^5\text{-}C_5H_5)$[85] (**2**) and $WIr_3(CO)_{11}(\eta^5\text{-}C_5H_4Me)$,[90] which show only terminal carbonyl groups. The number of bands in the ν(CO) region is indicative of the presence of isomers; the less-sterically hindered **8** has two extra bands in its IR spectrum which are not present in the spectra of **9** and **10**. In general the ν(CO) bands move to lower energy on progressing to the more substituted cyclopentadienyl groups, most evident in the bridging carbonyl region because the bridging coordination modes are more effective at removing electron density from the metal core. The ^{1}H NMR signals move to higher field as the number of methyl groups increases, most markedly for the ring proton resonances of **5**−**7**. The SI mass spectra contain peaks corresponding to the molecular ion and successive loss of carbonyl ligands, competitive with loss of methyl groups for **6**−**10**. The UV−vis spectra are featureless, with no distinct maxima, merely shoulders observed in the range 240−1000 nm.

Crystal Structures of 7 and 10. The molecular structures of **7** and **10** as determined by single-crystal X-ray studies are consistent with the formulations given above and, together with the previously reported structures of **1**[85] and **3**,[91] provide the opportunity to assess the effect of steric crowding on metrical parameters and ligand coordination modes. Selected bond lengths and angles are listed in Tables 1 and 2, and a summary of crystal and refinement data is shown in Table 3. ORTEP plots showing the molecular geometry and atomic numbering schemes are shown in Figures 1 (**7**) and 2 (**10**).

The complex **7** has the $MoIr_3$ pseudotetrahedral core geometry of the analogue $MoIr_3(\mu\text{-}CO)_3(CO)_8(\eta^5\text{-}C_5H_5)$ (**1**),[85] with a η^5-C_5Me_5 group ligating the molybdenum atom. Bridging carbonyls span the edges of a $MoIr_2$ face, and the remaining eight carbonyls bond in a terminal fashion, with two terminal carbonyls on each of Ir1 and Ir2, three terminal carbonyls on

(85) Churchill, M. R.; Li, Y.-J.; Shapley, J. R.; Foose, D. S.; Uchiyama, W. S. *J. Organomet. Chem.* **1986**, *312*, 121.
(86) King, R. B.; Stone, F. G. A. *Inorg. Synth.* **1963**, *7*, 107.
(87) Lucas, N. T.; Humphrey, M. G.; Hockless, D. C. R. *J. Organomet. Chem.* **1997**, *535*, 175.
(88) Shapley, J. R.; Hardwick, S. J.; Foose, D. S.; Stucky, G. D. *J. Am. Chem. Soc.* **1981**, *103*, 7383.
(89) Lucas, N. T.; Notaras, E. G. A.; Humphrey, M. G. *Acta Crystallogr.* **2001**, *E57*, m132.
(90) Notaras, E. G. A.; Lucas, N. T.; Blitz, J. P.; Humphrey, M. G. *J. Organomet. Chem.* **2001**, *631*, 143.
(91) Lucas, N. T.; Humphrey, M. G.; Healy, P. C.; Williams, M. L. *J. Organomet. Chem.* **1997**, *545*−*546*, 519.

Table 1. Selected Bond Lengths and Angles for $MoIr_3(\mu\text{-}CO)_3(CO)_8(\eta^5\text{-}C_5Me_5)$ (**7**)

Ir1−Ir2	2.701(1)	Mo4−C24	2.16(2)
Ir1−Ir3	2.705(1)	Ir1−C11	1.86(2)
Ir2−Ir3	2.704(1)	Ir1−C15	1.84(2)
Ir1−Mo4	2.869(2)	Ir2−C21	1.90(2)
Ir2−Mo4	2.865(2)	Ir2−C22	1.87(3)
Ir3−Mo4	2.910(2)	Ir3−C31	1.93(2)
Ir1−C12	2.10(2)	Ir3−C32	1.92(2)
Ir1−C14	2.15(2)	Ir3−C33	1.87(3)
Ir2−C12	2.10(2)	Ir3···C41	2.83(2)
Ir2−C24	2.21(2)	Mo4−C41	1.96(2)
Mo4−C14	2.09(2)	Mo4−Cp[a]	2.016
Ir2−Ir1−Ir3	60.03(3)	Ir1−Ir3−Ir2	59.92(3)
Ir2−Ir1−Mo4	61.82(4)	Ir1−Ir3−Mo4	61.31(4)
Ir3−Ir1−Mo4	62.87(4)	Ir2−Ir3−Mo4	61.23(3)
Ir1−Ir2−Ir3	60.05(3)	Ir1−Mo4−Ir2	56.22(4)
Ir1−Ir2−Mo4	61.96(4)	Ir1−Mo4−Ir3	55.82(4)
Ir3−Ir2−Mo4	62.93(4)	Ir2−Mo4−Ir3	55.84(3)

[a] Cp = centroid of the pentamethylcyclopentadienyl ring.

Table 2. Selected Bond Lengths and Angles for $Mo_2Ir_2(\mu\text{-}CO)_3(CO)_7(\eta^5\text{-}C_5Me_5)_2$ (**10**)

Ir1−Ir2	2.7087(8)	Ir1−C11	1.88(1)
Ir1−Mo3	2.889(1)	Ir1−C14	1.91(2)
Ir1−Mo4	2.853(1)	Ir2−C21	1.79(2)
Ir2−Mo3	2.858(1)	Ir2−C22	1.91(2)
Ir2−Mo4	2.895(1)	Ir2···C41	2.86(2)
Mo3−Mo4	3.141(2)	Ir2···C42	3.01(1)
Ir1−C12	2.08(2)	Mo3−C31	1.92(1)
Ir1−C13	2.13(2)	Mo4···C31	2.95(1)
Ir2−C12	2.10(2)	Mo4−C41	1.97(2)
Ir2−C23	2.24(1)	Mo4−C42	1.95(1)
Mo3−C13	2.14(1)	Mo3−Cp[a]	2.021
Mo3−C23	2.05(1)	Mo4−Cp[a]	2.049
Ir2−Ir1−Mo3	61.31(3)	Ir1−Mo3−Ir2	56.24(3)
Ir2−Ir1−Mo4	62.66(3)	Ir1−Mo3−Mo4	56.29(3)
Mo3−Ir1−Mo4	66.33(3)	Ir2−Mo3−Mo4	57.46(3)
Ir1−Ir2−Mo3	62.45(3)	Ir1−Mo4−Ir2	56.22(3)
Ir1−Ir2−Mo4	61.11(3)	Ir1−Mo4−Mo3	57.38(3)
Mo3−Ir2−Mo4	66.19(3)	Ir2−Mo4−Mo3	56.35(3)

[a] Cp = centroid of the pentamethylcyclopentadienyl ring.

Ir3, and one terminal carbonyl on the molybenum. The metal core bond distances of **7** ($Ir-Ir_{av}$ = 2.703 Å, $Ir-Mo_{av}$ = 2.881 Å) are slightly longer than those of **1** ($Ir-Ir_{av}$ = 2.700 Å, $Ir-Mo_{av}$ = 2.859 Å); the nonbridged Ir3−Mo4 bond [2.910(2) Å] is significantly longer than the other two carbonyl-bridged Ir−Mo bonds [2.865(2)/2.869(2) Å]. Proceeding from **1** to **7** thus results in core expansion. The pentamethylcyclopentadienyl group of **7** is inclined toward the $MoIr_2$ face spanned by the bridging carbonyl ligands, and is trans to the long Ir3−Mo4 bond. The carbonyls bridging the Ir−Mo bonds of **7** are more unsymmetrically disposed than are those of **1**, moving *closer* to the molybdenums, suggesting that electronic factors dominate over steric considerations for this ligand disposition. The Mo4-bound carbonyl CO41 has a semi-bridging interaction[92] with Ir3 [Mo4−C41−O41 = 170(2)°, Ir3···C41 = 2.83(2) Å, asymmetry parameter[93,94] α = 0.44].

Complex **10** has the dimolybdenum−diiridium pseudotetrahedral core geometry of the cyclopentadienyl-containing analogue $Mo_2Ir_2(CO)_{10}(\eta^5\text{-}C_5H_5)_2$ (**3**),[87] with $\eta^5\text{-}C_5Me_5$ groups ligating both molybdenum atoms. Bridging carbonyls span the edges of a $MoIr_2$ face, and the remaining seven carbonyls bond in a terminal fashion: two terminal carbonyls on each of Ir1 and Ir2, one terminal carbonyl on Mo3, and two terminal carbonyls on Mo4 complete the coordination. As above, introduction of sterically demanding, and more electron-donating, ligands results in core expansion: the metal core bond distances of **10** [Ir−Ir = 2.7087(8) Å, $Ir-Mo_{av}$ = 2.874 Å, Mo−Mo = 3.141(2) Å] are significantly longer than those of **3** [Ir−Ir = 2.6972(9) Å, $Ir-Mo_{av}$ = 2.856 Å, Mo−Mo = 3.111(1) Å], with the Mo−Mo bond showing the greatest difference as would be expected on steric grounds. The longest Mo−Ir bond is trans to the $\eta^5\text{-}C_5Me_5$ group on Mo4 [Mo4−Ir2 = 2.895(1) Å]; the shortest Mo−Ir bond is the other nonbridged Ir−Mo4 vector [Mo4−Ir1 = 2.853(1) Å]. The pentamethylcyclopentadienyl group on Mo3 is inclined toward the $MoIr_2$ face spanned by the bridging carbonyl ligands. As was seen for **7**, the carbonyls bridging Ir−Mo bonds of **10** (α_{av} = 0.05) are more unsymmetrically disposed than are those of the cyclopentadienyl-ligated analogue (α_{av} = 0.01). The same electronic factors probably explain the presence of semi-bridging interactions for the three molybdenum-bound carbonyl groups CO31 (α = 0.54), CO41 (α = 0.45), and CO42 (α = 0.54), which likely help distribute electron density to the other metals. In addition, CO13 is tilted toward Mo4 with Mo4···C13 = 2.99(1) Å (Ir1−C13···Mo4, α = 0.40; Mo3−C13···Mo4, α = 0.40) affording an unusual "semi-face-capping" carbonyl ligand, also observed for **3**.[87]

Table 3. Crystal Data for **7**, **10**, and **13**

	7	10	13
formula	$C_{21}H_{15}Ir_3MoO_{11}$	$C_{30}H_{30}Ir_2Mo_2O_{10}$	$C_{19}H_{16}Ir_3O_{10}PW$
fw	1115.94	1126.88	1195.81
crystal size (mm^3)	0.40 × 0.08 × 0.06	0.70 × 0.50 × 0.50	0.35 × 0.29 × 0.18
color, habit	orange, needle	red-brown, block	orange, fragment
T (K)	296	296	200
diffractometer	Rigaku AFC6S	Rigaku AFC6S	Nonius KappaCCD
crystal system	monoclinic	tetragonal	triclinic
space group	$P2_1/c$ (#14)	$P4_12_12$ (#92)	$P\bar{1}$ (#2)
a (Å)	8.523(4)	16.332(2)	9.2819(1)
b (Å)	19.434(3)		9.6886(1)
c (Å)	15.469(3)	24.696(5)	14.9537(2)
α (deg)			81.7838(5)
β (deg)	91.84(2)		72.8327(5)
γ (deg)			68.1183(8)
V ($Å^3$)	2561(1)	6587(2)	1191.46(3)
Z	4	8	2
D_{calc} (g cm^{-3})	2.89	2.272	3.33
F(000)	2008	4224	1060
μ_{Mo} (mm^{-1})	16.012	8.873	21.684
θ_{max} (deg)	25.05	25.05	30.05
index ranges	$0 \le h \le 10$	$-19 \le h \le 19$	$-13 \le h \le 12$
	$0 \le k \le 23$	$-19 \le k \le 19$	$-13 \le k \le 13$
	$-18 \le l \le 18$	$-29 \le l \le 29$	$-21 \le l \le 21$
$N_{measured}$	5026	3396	28946
N_{unique}	4695	3366	6967
N_{obs} ($I > 2\sigma(I)$)	3229	2835	6038
absorp corr	ψ-scan	ψ-scan	integration
T_{min}, T_{max}	0.14, 0.38	0.007, 0.012	0.039, 0.11
N_{param}	326	398	308
R ($I > 2\sigma(I)$)[a]	0.044	0.033	0.048
R_w ($I > 2\sigma(I)$)[b]	0.051	0.034	0.057
GOF	2.17	1.59	1.41
largest diff peak, hole (e $Å^{-3}$)	2.22, −2.51	1.25, −1.66	6.07, −5.56

[a] $R = \sum||F_o| - |F_c||/\sum|F_o|$. [b] $R_w = [(\sum w(|F_o| - |F_c|)^2/\sum wF_o^2]^{1/2}$, $w = [\sigma_c^2(F_o) + 0.0001(F_o^2)]^{-1}$.

Reactions of $WIr_3(CO)_{11}(\eta^5\text{-}C_5H_4Me)$ (11) and $W_2Ir_2(CO)_{10}(\eta^5\text{-}C_5H_4Me)_2$ (12) with PMe_3. The reactions of $WIr_3(CO)_{11}(\eta^5\text{-}C_5H_4Me)$ (**11**) or $W_2Ir_2(CO)_{10}(\eta^5\text{-}C_5H_4Me)_2$ (**12**) with

(92) Cotton, F. A.; Kruczynski, L.; Frenz, B. A. *J. Organomet. Chem.* **1978**, *160*, 93.
(93) Klingler, R. J.; Butler, W. M.; Curtis, M. D. *J. Am. Chem. Soc.* **1978**, *100*, 5034.
(94) Curtis, M. D.; Han, K. R.; Butler, W. M. *Inorg. Chem.* **1980**, *19*, 2096.

Scheme 3. Syntheses of $WIr_3(CO)_{10}(PMe_3)(\eta^5\text{-}C_5H_4Me)$ (**13**), $WIr_3(CO)_9(PMe_3)_2(\eta^5\text{-}C_5H_4Me)$ (**14**), $W_2Ir_2(CO)_9(PMe_3)(\eta^5\text{-}C_5H_4Me)_2$ (**15**), and $W_2Ir_2(CO)_8(PMe_3)_2(\eta^5\text{-}C_5H_4Me)_2$ (**16**)

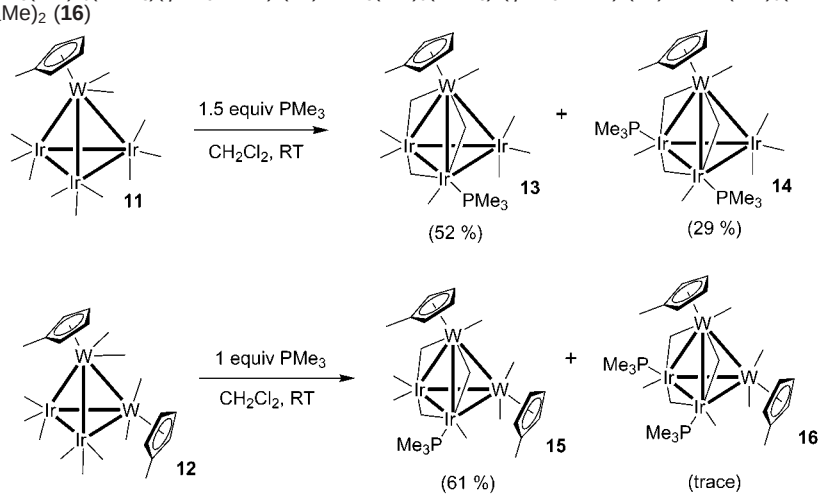

1−1.5 equiv of PMe_3 proceed in dichloromethane at room temperature to afford monosubstitution products $WIr_3(CO)_{10}(PMe_3)(\eta^5\text{-}C_5H_4Me)$ (**13**) and $W_2Ir_2(CO)_9(PMe_3)(\eta^5\text{-}C_5H_4Me)_2$ (**15**) as major products in good yield (Scheme 3). In addition, the bis-substitution products $WIr_3(CO)_9(PMe_3)_2(\eta^5\text{-}C_5H_4Me)$ (**14**) and $W_2Ir_2(CO)_8(PMe_3)_2(\eta^5\text{-}C_5H_4Me)_2$ (**16**) were isolated in lower yield from the respective reactions; neither was sufficiently stable to afford acceptable analytical data, and **16** was insufficiently stable to be used in further studies. The clusters **13**−**15** have been characterized by a combination of IR and ^{1}H NMR spectroscopies, SI mass spectrometry, and satisfactory microanalysis (**13** and **15** only), while the unstable product **16** has been characterized by IR and ^{1}H NMR spectroscopies only. The spectroscopic features of **13**−**16** are similar to those of their cyclopentadienyl analogues,[95,96] but extra bands are observed in the solution IR spectra of some examples.

Crystal Structure of 13. The molecular structure of **13** as determined by single-crystal X-ray studies is consistent with the formulation given above and defines the substitution site of the phosphine. A summary of crystal and refinement data is shown in Table 3, and selected bond lengths and angles are listed in Table 4. An ORTEP plot showing the molecular geometry and atomic numbering scheme is shown in Figure 3.

The complex **13** has the WIr_3 pseudotetrahedral framework of the precursor cluster $WIr_3(CO)_{11}(\eta^5\text{-}C_5H_4Me)$ (**11**).[89] The tungsten atom is ligated by a methylcyclopentadienyl group, a trimethylphosphine ligates Ir1, three bridging carbonyls span the Ir1−Ir2−W3 face, and seven terminal carbonyl ligands complete the coordination sphere. The core distances fall into the ranges Ir−Ir [2.6804(5)−2.7395(4); $Ir-Ir_{av}$ = 2.708 Å] and Ir−W [2.8013(4)−2.9013(5); $Ir-W_{av}$ = 2.851 Å], and are on average shorter than those of the cyclopentadienyl analogue $WIr_3(\mu\text{-}CO)_3(CO)_7(PMe_3)(\eta^5\text{-}C_5H_5)$ [$Ir-Ir_{av}$ = 2.745 Å, $Ir-W_{av}$ = 2.858 Å].[95] Comparison with the structure of the precursor cluster **11** [$Ir-Ir_{av}$ = 2.700 Å, $Ir-W_{av}$ = 2.823 Å][89] indicates a slight lengthening of the core bonds, a trend consistent with previously studied substituted tungsten−iridium clusters.[70,95,97] Note that the precursor cluster has an all-terminal carbonyl configuration; this change in carbonyl bonding following phosphine substitution is not unprecedented, having also been observed for the analogous cyclopentadienyl cluster $WIr_3(\mu\text{-}CO)_3(CO)_7(PMe_3)(\eta^5\text{-}C_5H_5)$.[95] However, in the cyclopentadienyl-containing example the carbonyls bridge an Ir_3 plane, whereas in **13** the bridging occurs around a WIr_2 plane. Relative to the plane of bridging carbonyls, the phosphine in **13** coordinates in a radial site ($\eta^5\text{-}C_5H_4Me$ axial), whereas the phosphine ligates axially ($\eta^5\text{-}C_5H_5$ apical) in $WIr_3(\mu\text{-}CO)_3(CO)_7(PMe_3)(\eta^5\text{-}C_5H_5)$. Both of these coordination geometries have been suggested for isomers present in solution observed in NMR fluxionality studies of $WIr_3(\mu\text{-}CO)_3(CO)_7(PMe_3)(\eta^5\text{-}C_5H_5)$,[98] but the present study provides the first solid-state evidence for this configuration. The tungsten-bound carbonyl CO31 has a semi-bridging interaction with Ir4 [$\angle W3-C31-O31$ = 172.8(9)°, $Ir4\cdots C31$ = 2.914(9)°, α = 0.48].

Table 4. Selected Bond Lengths and Angles for $WIr_3(\mu\text{-}CO)_3(CO)_7(PMe_3)(\eta^5\text{-}C_5H_4Me)$ (**13**)

Ir1−Ir2	2.6804(5)	W3−C2	2.085(9)
Ir1−Ir4	2.7395(4)	W3−C3	2.172(9)
Ir2−Ir4	2.7043(5)	Ir1−C11	1.876(9)
Ir1−W3	2.8013(4)	Ir2−C21	1.89(1)
Ir2−W3	2.8517(5)	Ir2−C22	1.883(9)
Ir4−W3	2.9013(5)	Ir4−C41	1.920(9)
Ir1−P1	2.317(2)	Ir4−C42	1.882(9)
Ir1−C1	2.057(9)	Ir4−C43	1.95(1)
Ir1−C3	2.092(9)	W3−C31	1.967(9)
Ir2−C1	2.170(9)	W3−Cp[a]	1.989
Ir2−C2	2.190(9)		
Ir2−Ir1−Ir4	59.85(1)	Ir1−Ir4−Ir2	58.99(1)
Ir2−Ir1−W3	62.65(1)	Ir1−Ir4−W3	59.47(1)
Ir4−Ir1−W3	63.14(1)	Ir2−Ir4−W3	61.04(1)
Ir1−Ir2−Ir4	61.16(1)	Ir1−W3−Ir2	56.60(1)
Ir1−Ir2−W3	60.75(1)	Ir1−W3−Ir4	57.39(1)
Ir4−Ir2−W3	62.89(1)	Ir2−W3−Ir4	56.07(1)

[a] Cp = centroid of the pentamethylcyclopentadienyl ring.

Raman Spectroscopy. Low-frequency Raman spectra for clusters **5**, **8**, **11**, and **12** are displayed in Figure 4, together with that of the homometallic tetrahedral cluster $Ir_4(CO)_{12}$, the data from which has been reported in an earlier study;[76] the observed Raman frequencies are presented in Table 5 together with symmetries of these vibrational modes. Three intense bands at 207, 161, and 131 cm^{-1} have been assigned previously to

(95) Waterman, S. M.; Humphrey, M. G.; Tolhurst, V.-A.; Skelton, B. W.; White, A. H.; Hockless, D. C. R. *Organometallics* **1996**, *15*, 934.
(96) Waterman, S. M.; Humphrey, M. G.; Lee, J.; Ball, G. E.; Hockless, D. C. R. *Organometallics* **1999**, *18*, 2440.
(97) Waterman, S. M.; Humphrey, M. G.; Hockless, D. C. R. *J. Organomet. Chem.* **1998**, *565*, 81.
(98) Waterman, S. M.; Humphrey, M. G. *Organometallics* **1999**, *18*, 3116.

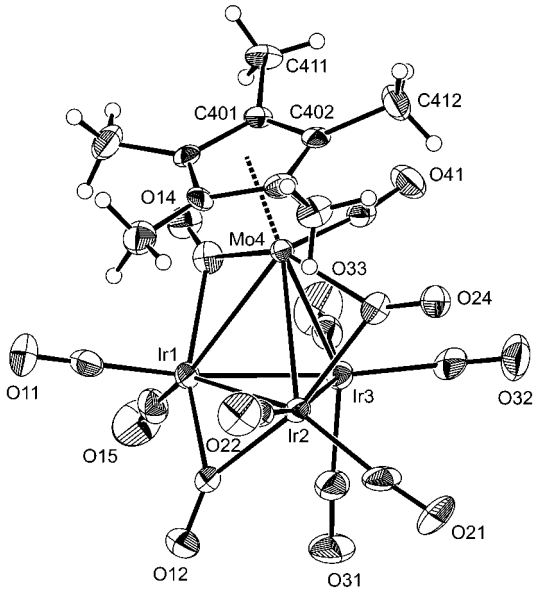

Figure 1. Molecular structure and atomic numbering scheme for $MoIr_3(\mu\text{-}CO)_3(CO)_8(\eta^5\text{-}C_5Me_5)$ (**7**). Displacement ellipsoids are shown at the 30% probability level; hydrogens have an arbitrary radius.

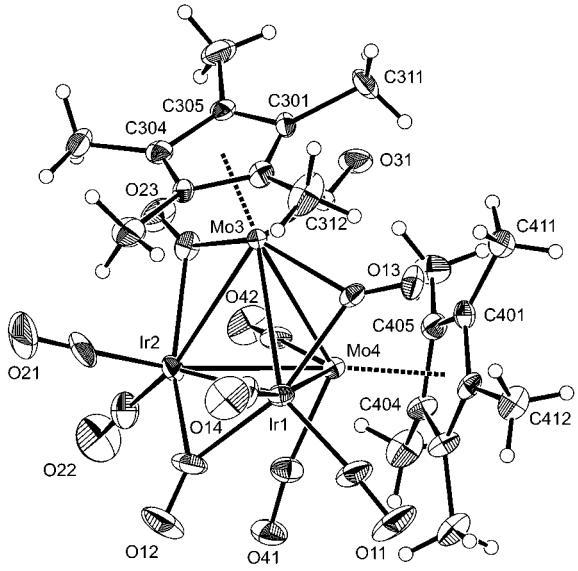

Figure 2. Molecular structure and atomic numbering scheme for $Mo_2Ir_2(\mu\text{-}CO)_3(CO)_7(\eta^5\text{-}C_5Me_5)_2$ (**10**). Displacement ellipsoids are shown at the 30% probability level; hydrogens have an arbitrary radius.

the anticipated cluster modes of A_1, T_2, and E symmetries, respectively.[76] The idealized symmetry of $Ir_4(CO)_{12}$ (T_d) is reduced to C_s on proceeding to the cyclopentadienyl-containing clusters **1**−**4**, and the methylcyclopentadienyl-containing clusters **5**, **11**, **8**, and **12**. The metal cores of the $[MIr_3]$ (**1**, **2**, **5**, **11**) and $[M_2Ir_2]$ (**3**, **4**, **8**, **12**) clusters have C_{3v} or C_{2v} symmetry, respectively. Instrumental limitations have precluded examination of the low-energy E mode for $Ir_4(CO)_{12}$, but the frequencies of the A_1 and T_2 modes are reproduced in the current study. The T_2 mode of T_d transforms to A_1 and E modes in the C_{3v} point group and $A_1 + B_1 + B_2$ modes in the C_{2v} point group; in C_{2v}, 4 M−M modes are possible. The low-frequency region of the Raman spectra for carbonyl clusters typically contain bands corresponding to metal−metal stretching and metal−carbon deformation modes, but previous studies have found limited mode-mixing,[75,76] justifying a correlation between the

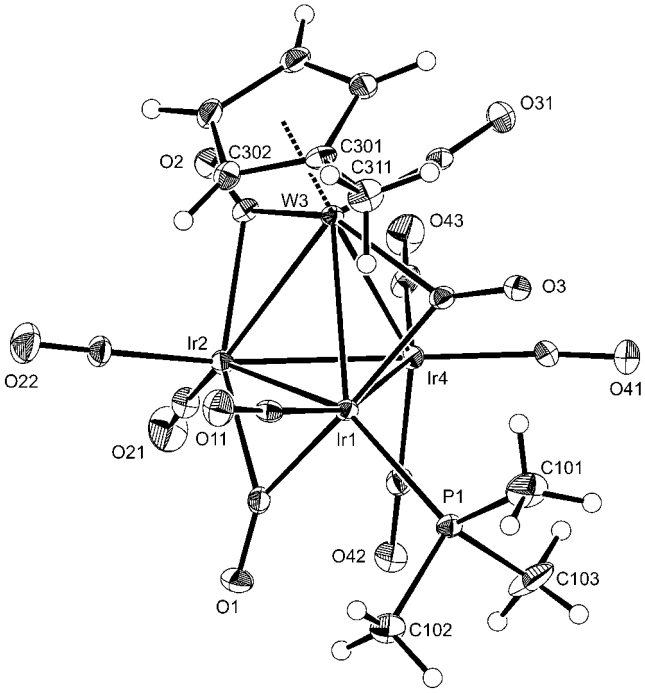

Figure 3. Molecular structure and atomic numbering scheme for $WIr_3(\mu\text{-}CO)_3(CO)_7(PMe_3)(\eta^5\text{-}C_5H_4Me)$ (**13**). Displacement ellipsoids are shown at the 30% probability level; hydrogens have an arbitrary radius.

tabulated frequencies and average cluster core bond strengths. Specifically, frequencies for the A_1 breathing mode decrease on proceeding from $Ir_4(CO)_{12}$ to **5**, **11** and then to **8**, **12**, corresponding to increasing incorporation of group 6 metal into the cluster core, and consistent with the trend in metal−metal distances [Ir−Ir < M−Ir < M−M]. Proceeding from **11** to **5** results in significant broadening of the 194 cm^{-1} band, and proceeding from **12** to **8** results in some broadening of the 176/183 cm^{-1} band. As replacing tungsten by molybdenum in these clusters results in the solid-state cluster structure changing from an all-terminal carbonyl geometry to one in which there is a plane of bridging carbonyls, it seems likely that this broadening reflects this molecular modification rather than intermolecular factor group splitting.

Redox Behavior of $[MIr_3]$ Clusters (M = Mo, W). All clusters considered in the present study are electron precise (60 CVE) in the resting state. The cyclic voltammetric scans of the tetrahedral complexes $MoIr_3(CO)_{11}(\eta^5\text{-}C_5H_{5-n}Me_n)$ [$n = 0$ (**1**), 1 (**5**), 4 (**6**), and 5 (**7**)], $WIr_3(CO)_{11}(\eta^5\text{-}C_5H_4Me)$ (**11**), and $WIr_3(CO)_{10}(PMe_3)(\eta^5\text{-}C_5H_4Me)$ (**13**), using a switching potential of 1.7 V, show two successive irreversible oxidative waves of equal peak current height [Table 6: a representative CV (that of **6**) is displayed in Figure 5]. The bis-phosphine substitution product $WIr_3(CO)_9(PMe_3)_2(\eta^5\text{-}C_5H_4Me)$ (**14**) exhibits a third irreversible oxidative wave in this region. Replacement of the cyclopentadienyl group of **1** with methyl-substituted cyclopentadienyl groups (**5**−**7**) results in a decrease in first oxidation potential, as would be expected for the introduction of electron-donating methyl groups. Likewise, the substitution of CO in **11** by the strongly electron-donating PMe_3 ligand (clusters **13** and **14**) results in a decrease in the oxidation potentials. No significant increases in reversibility were noted for these $[MIr_3]$ clusters, even when the scan rate was increased (up to 1600 mV s^{-1}) and the solution was cooled to −20 °C. Small daughter peaks arising from decomposition products are seen at G and H.

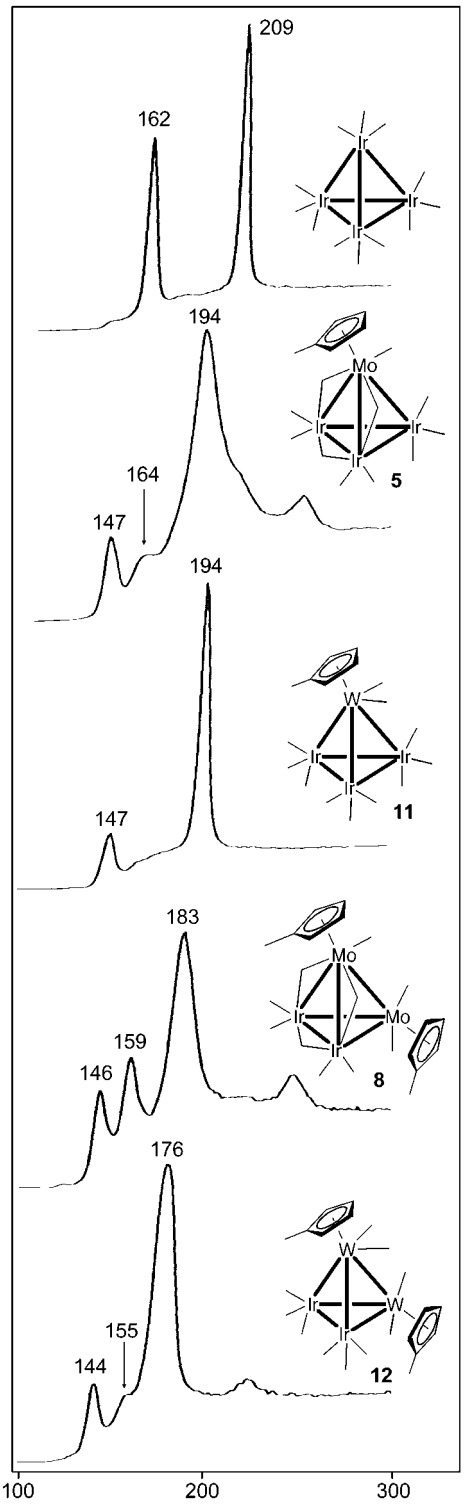

Figure 4. Low-frequency Raman spectra (cm^{-1}) for solid samples of $Ir_4(CO)_{12}$, $MoIr_3(\mu\text{-}CO)_3(CO)_8(\eta^5\text{-}C_5H_4Me)$ (**5**), $Mo_2Ir_2(\mu\text{-}CO)_3(CO)_7(\eta^5\text{-}C_5H_4Me)_2$ (**8**), $WIr_3(CO)_{11}(\eta^5\text{-}C_5H_4Me)$ (**11**), and $W_2Ir_2(CO)_{10}(\eta^5\text{-}C_5H_4Me)_2$ (**12**).

Attempts to quantify the electron transfer stoichiometry for the first oxidation process using controlled potential coulometry were inconclusive; this oxidation has tentatively been assigned as a one-electron process.

A single irreversible one-electron reduction process (A) is observed for all seven clusters **1**, **5**−**7**, **11**, **13**, and **14** (Figure 5, Table 6) for a switching potential of −1.7 V. No increases in reversibility were detected on increasing the scan rate or cooling the solution. Peaks corresponding to oxidation of the species arising from the irreversible reductive process are present in the reverse sweep (B−E). The relative ordering of reduction potentials for these clusters is identical with that seen for the oxidation processes; the most easily oxidized cluster is also the most difficult to reduce (and the most difficult to oxidize is the easiest to reduce). The tungsten-containing cluster **11** is easier to oxidize (and harder to reduce) than its molybdenum-containing analogue **5** (a difference of 230 mV between first oxidation potentials and 40 mV between reduction potentials).

Table 5. Observed Low-Frequency Raman Bands (cm^{-1}) and Assignments for $Ir_4(CO)_{12}$, $MoIr_3(\mu\text{-}CO)_3(CO)_8(\eta^5\text{-}C_5H_4Me)$ (**5**), $Mo_2Ir_2(\mu\text{-}CO)_3(CO)_7(\eta^5\text{-}C_5H_4Me)_2$ (**8**), $WIr_3(CO)_{11}(\eta^5\text{-}C_5H_4Me)$ (**11**), and $W_2Ir_2(CO)_{10}(\eta^5\text{-}C_5H_4Me)_2$ (**12**)

	Raman bands (cm^{-1})	
cluster	A_1	T_2 (or lower symmetry components)
$Ir_4(CO)_{12}$	209	162
$WIr_3(CO)_{11}(\eta^5\text{-}C_5H_4Me)$ (**11**)	194	147
$MoIr_3(\mu\text{-}CO)_3(CO)_8(\eta^5\text{-}C_5H_4Me)$ (**5**)	194	164, 147
$W_2Ir_2(CO)_{10}(\eta^5\text{-}C_5H_4Me)_2$ (**12**)	176	155, 144
$Mo_2Ir_2(\mu\text{-}CO)_3(CO)_7(\eta^5\text{-}C_5H_4Me)_2$ (**8**)	183	159, 146

Redox Behavior of [M_2Ir_2] Clusters (M = Mo, W). The cyclic voltammetric scans of the tetrahedral complexes $Mo_2Ir_2(CO)_{10}(\eta^5\text{-}C_5H_{5-n}Me_n)_2$ [$n = 0$ (**3**), 1 (**8**), 4 (**9**), and 5 (**10**)], $W_2Ir_2(CO)_{10}(\eta^5\text{-}C_5H_4Me)_2$ (**12**), and $W_2Ir_2(CO)_9(PMe_3)(\eta^5\text{-}C_5H_4Me)_2$ (**15**), using a switching potential of 1.7 V, show two successive one-electron oxidation waves [Table 6: a representative CV (that of **8**) is displayed in Figure 6]. The first process (D/d) is reversible or quasireversible, while the second process (E) is irreversible except in the case of **15**, for which the electron-donating PMe_3 group appears to stabilize the dicationic species and a partially reversible process is observed (Figure 7). Replacement of the cyclopentadienyl groups of **3** with methyl-substituted cyclopentadienyl groups (**8**−**10**) results in a decrease in both oxidation potentials, the same trend that is seen for the related [$MoIr_3$] clusters discussed above; the presence of two ($\eta^5\text{-}C_5H_{5-n}Me_n$) groups in **3**, **8**−**10** makes the effect more pronounced. The substitution of one CO on **12** by PMe_3 to give **15** results in an increase in the ease of oxidation by 190 mV, approximately twice that seen for the corresponding [WIr_3] clusters **11** and **13** ($\Delta E = 90$ mV). No significant increases in reversibility for the second oxidation process of the molybdenum-containing clusters were noted when the scan rate was increased and the solution was cooled to −20 °C. The electron-transfer stoichiometry for the reversible, first oxidation of **12** has been quantified as a one-electron process using controlled potential coulometry.

The first reduction process (A) observed for clusters **3**, **8**−**10**, **12**, and **15** is irreversible and involves the transfer of two electrons by peak height comparison (Figure 6). When the switching potential was increased to −2.0 V, a second irreversible process was detected for **9** and **10**. Increasing the scan rate or cooling the solution had no effect on the reversibility of either reduction process. At higher scan rates the largest daughter peak (C) in the reverse scan increased in size relative to the forward peaks, indicative of a lifetime of the order of seconds for this decomposition intermediate.

As was seen for the [MIr_3] clusters above, the tungsten-containing cluster **12** is more easily oxidized (or more difficult to reduce) than its molybdenum-containing analogue **8**, although

Table 6. Cyclic Voltammetric Data (V) for **1**, **3**, and **5**−**15**

	oxidations[a]			reductions[a]	
$MoIr_3(CO)_{11}(\eta^5\text{-}C_5H_5)$ (**1**)		1.55	1.32 (1e)	−1.15 (1e)	
$MoIr_3(CO)_{11}(\eta^5\text{-}C_5H_4Me)$ (**5**)		1.54	1.29 (1e)	−1.27 (1e)	
$MoIr_3(CO)_{11}(\eta^5\text{-}C_5HMe_4)$ (**6**)		1.58	1.24 (1e)	−1.30 (1e)	
$MoIr_3(CO)_{11}(\eta^5\text{-}C_5Me_5)$ (**7**)		1.49	1.23 (1e)	−1.33 (1e)	
$WIr_3(CO)_{11}(\eta^5\text{-}C_5H_4Me)$ (**11**)		1.27	1.06 (1e)	−1.31 (1e)	
$WIr_3(CO)_{10}(PMe_3)(\eta^5\text{-}C_5H_4Me)$ (**13**)		1.38	0.97 (1e)	−1.50 (1e)	
$WIr_3(CO)_9(PMe_3)_2(\eta^5\text{-}C_5H_4Me)$ (**14**)	1.23	0.75	0.65 (1e)	−1.81 (1e)	
$Mo_2Ir_2(CO)_{10}(\eta^5\text{-}C_5H_5)_2$ (**3**)		1.07	0.84 [160][b] (1e)	−1.24 (2e)	
$Mo_2Ir_2(CO)_{10}(\eta^5\text{-}C_5H_4Me)_2$ (**8**)		1.05	0.82 [80][b] (1e)	−1.23 (2e)	(−1.70)
$Mo_2Ir_2(CO)_{10}(\eta^5\text{-}C_5HMe_4)_2$ (**9**)		1.00	0.71 [130][b] (1e)	−1.37 (2e)	−1.86
$Mo_2Ir_2(CO)_{10}(\eta^5\text{-}C_5Me_5)_2$ (**10**)		1.02	0.71 [120][b] (1e)	−1.33 (2e)	−1.85
$W_2Ir_2(CO)_{10}(\eta^5\text{-}C_5H_4Me)_2$ (**12**)		1.00	0.70 [70][b] (1e)	−1.50 (2e)	
$W_2Ir_2(CO)_9(PMe_3)(\eta^5\text{-}C_5H_4Me)_2$ (**15**)		0.74 [70][b] (1e)	0.51 [60][b] (1e)	−1.68 (2e)	

[a] All clusters exhibit irreversible processes except where indicated. [b] Partially reversible $E_{1/2}$ [$E_pf - E_pr$ (mV)].

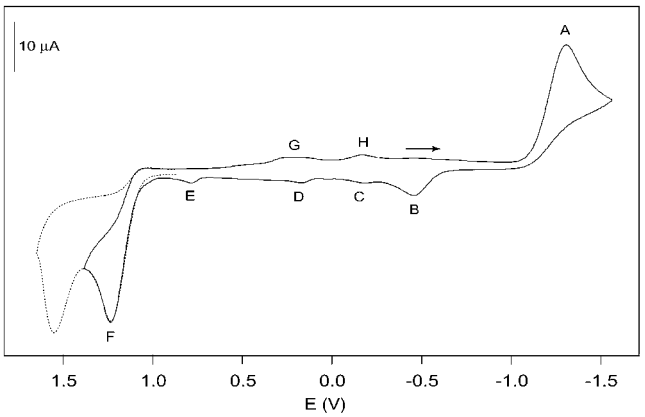

Figure 5. Cyclic voltammogram of 5.1×10^{-3} M $MoIr_3(CO)_{11}(\eta^5\text{-}C_5HMe_4)$ (**6**) in CH_2Cl_2 with 0.25 M $(NBu^n_4)PF_6$ as supporting electrolyte (scan rate: 200 mV s^{-1}).

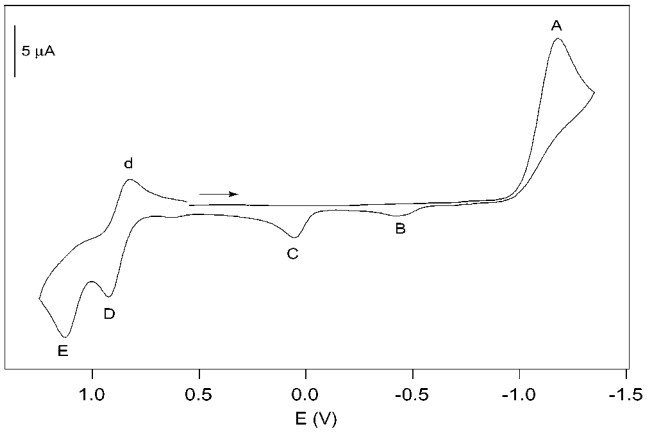

Figure 6. Cyclic voltammogram of 1.7×10^{-3} M $Mo_2Ir_2(CO)_{10}(\eta^5\text{-}C_5H_4Me)_2$ (**8**) in CH_2Cl_2 with 0.25 M $(NBu^n_4)PF_6$ as supporting electrolyte (scan rate: 200 mV s^{-1}).

in this case the greatest difference is seen in the reductive (ΔE = 270 mV) rather than oxidative (ΔE = 120 mV) behavior. The clusters $Mo_2Ir_2(CO)_{10}(\eta^5\text{-}C_5H_{5-n}Me_n)_2$ (**3**, **8**−**10**) are more easily oxidized than the respective clusters $MoIr_3(CO)_{11}(\eta^5\text{-}C_5H_{5-n}Me_n)$ (**1**, **5**−**7**).

Spectroelectrochemical Studies. The reversible one-electron oxidation of the $[M_2Ir_2]$ clusters has been probed. A typical example, $W_2Ir_2(CO)_{10}(\eta^5\text{-}C_5H_4Me)_2$ (**12**), was examined by UV−vis−NIR and IR spectroelectrochemistry. Electronic absorption spectra of the oxidation of **12** in an OTTLE cell are shown in Figure 8. Oxidation results in the isosbestic disappearance of bands centered at 21 500 and 35 000 cm^{-1} and simultaneous appearance of similar intensity bands at 18 000 and 37 000 cm^{-1}, together with a low-energy low-intensity band at 8 000 cm^{-1}. Few reports of UV−vis(−NIR) spectroelectrochemistry of transition metal carbonyl clusters are extant,[54,60,63] and no similar NIR transitions have been reported. Changes in the IR ν(CO) region on one-electron oxidation of **12** are shown in the difference spectra of Figure 9, obtained in a thin-layer reflectance cell. While the single-crystal X-ray structural study of **12**[99] reveals all-terminal carbonyl coordination, the solution IR spectrum is consistent with the presence of an isomer with bridging carbonyls [ν(CO) 1750−1900 cm^{-1}], possibly isostructural with the solid-state structure of $Mo_2Ir_2(\mu\text{-}CO)_3(CO)_7(\eta^5\text{-}C_5H_5)_2$ (**3**).[87] Oxidation results in progressive disappearance of the bridging carbonyl bands, accompanied by appearance of several strong bands in the terminal carbonyl ν(CO) region [ν(CO) 1950−2150 cm^{-1}]. Several transition metal carbonyl clusters have been examined by ν(CO) IR spectroelectro-

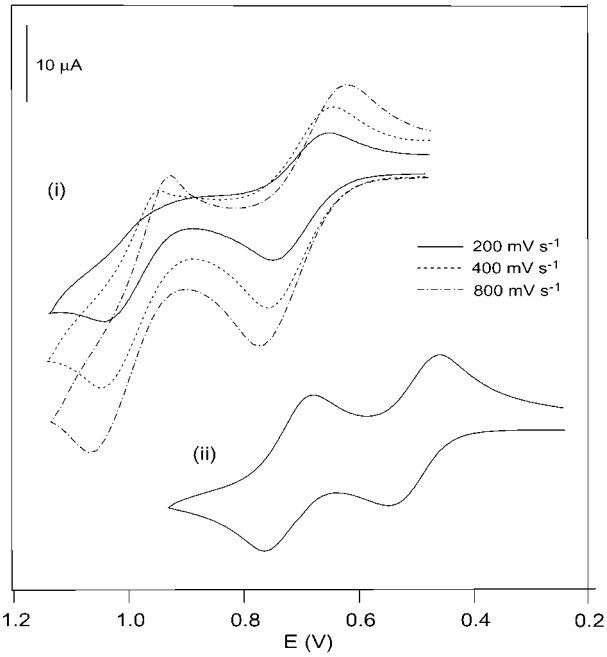

Figure 7. Cyclic voltammograms of (i) 2.0×10^{-3} M $W_2Ir_2(CO)_{10}(\eta^5\text{-}C_5H_4Me)_2$ (**12**) showing the effect of scan rate variation and (ii) 1.8×10^{-3} M $W_2Ir_2(CO)_9(PMe_3)(\eta^5\text{-}C_5H_4Me)_2$ (**15**) in CH_2Cl_2 with 0.25 M $(NBu^n_4)PF_6$ as supporting electrolyte.

(99) Lucas, N. T.; Notaras, E. G. A.; Humphrey, M. G. *Acta Crystallogr.* **2001**, *E57*, m132.

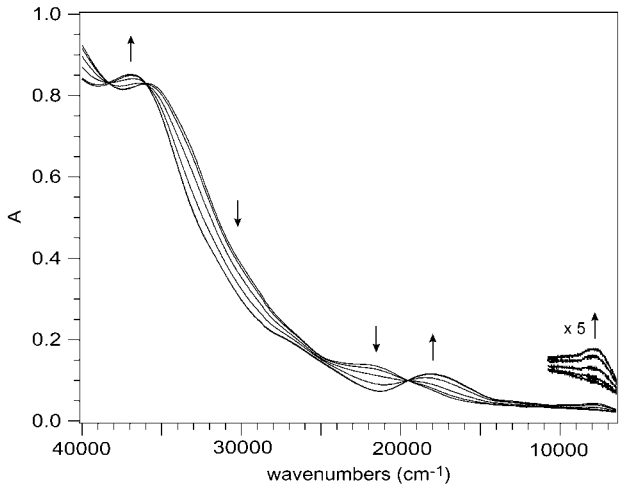

Figure 8. UV−vis−NIR spectra of $W_2Ir_2(CO)_{10}(\eta^5\text{-}C_5H_4Me)_2$ (**12**) [CH_2Cl_2, 0.25 M (NBu^n_4)PF_6] during exhaustive oxidation ($0 \rightarrow 1^+$) at $E_{appl} \approx$ 0.90 V at 233 K.

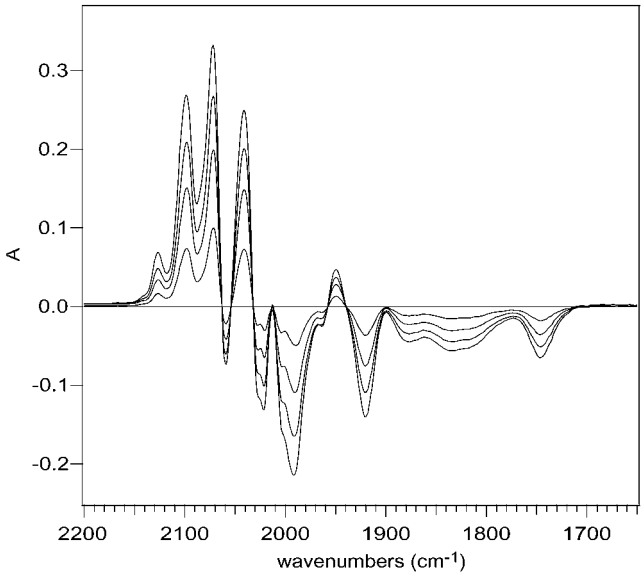

Figure 9. Changes in the IR difference spectrum of $W_2Ir_2(CO)_{10}(\eta^5\text{-}C_5H_4Me)_2$ (**12**) accompanying the oxidation ($0 \rightarrow 1^+$) at $E_{appl} \approx$ 0.90 V at 233 K [CH_2Cl_2, 0.25 M (NBu^n_4)PF_6].

chemistry,[28,53,55−59,61−69] including an example of cluster reduction rearranging an all-terminal carbonyl coordination to one involving bridging ligands.[66] In the present studies, the isomer distribution in the resting state of all-terminal (crystallographically verified) and bridging-carbonyl (spectroscopically assigned) forms is displaced to purely all-terminal on cluster oxidation. This results from the decrease in $d\pi$(M)→$2\pi^*$(CO) back-bonding because of the decrease of electron density from cluster oxidation;[57] a similar example of an all-bridging isomer rearranging to an isomeric form with a terminal carbonyl on one-electron oxidation has been noted recently with tricobalt clusters.[67]

Computational Studies. Approximate density functional theory calculations have been carried out on the archetypal $W_2Ir_2(CO)_{10}(\eta^5\text{-}C_5H_5)_2$ (**4**), to rationalize observations from the electrochemical and spectroelectrochemical studies. Relative energies of the pertinent stationary points located for the +1, 0, and −2 charge states, calculated at the LDA/II and (B-LYP, ZORA)/IV//LDA/II[100] levels of theory, are summarized in Table 7. In analyzing first the optimized geometries of the uncharged species, we find that the LDA/II calculations indicate that the tetrahedral structure is thermodynamically unstable relative to a butterfly structure corresponding to cleavage of the W−W bond, with a difference in energy of almost 2 eV between these two structures. Calculations at the LDA/IV level yield a similar result, clearly at variance with the experimentally determined tetrahedral core structure for the neutral cluster. Inclusion of nonlocal and of scalar relativistic corrections (particularly the latter) reverses the relative energies, with the tetrahedral geometry now being favored by ca. 0.5 eV (though the barrier to interconversion between these two structures is expected to be significantly larger than this).

Table 7. Calculated Relative Energies for $[W_2Ir_2(CO)_{10}(\eta^5\text{-}C_5H_5)_2]^{n\pm}$ (**4**$^{n\pm}$)

	E_{rel} (eV)[a]		r(M–M′) (Å)[b]		
charge state	VWN/II	B-LYP+ZORA/ IV//VWN/II	W–W	W–Ir	Ir–Ir
+1	**8.03**	**6.57**	3.41	2.79	2.83
0	0	**0**	3.21	2.83	2.74
	−1.88	+0.49	5.05	2.98	2.88
−2	−2.88	+0.07	2.97	2.88	2.86
	−4.54	+0.08	5.02	2.95	2.72
	−5.82	**−1.31**	4.93	2.96	*3.28*
−2 (−CO)	−0.84	+1.47	3.01	2.78	2.95

[a] Bold entries are the most stable species. [b] Obtained using VWN/II. Underlined entries are nonbonding distances, italicized entries are borderline bonding/nonbonding.

Comparison of the various levels of theory with experiment is instructive. Spontaneous formation of the tetrahedral core of $W_2Ir_2(CO)_{10}(\eta^5\text{-}C_5H_5)_2$ under experimental synthesis conditions[88] suggests that this is the preferred, and therefore lowest energy, mode of $[W_2Ir_2]$ connectivity for this species: computationally, inclusion of relativistic corrections is required to reproduce this result. However, the inclusion of relativistic corrections also gives a somewhat *poorer* result in terms of optimized metal−metal bond lengths: when compared with the crystallographic data (W−W = 2.99 Å, Ir−Ir = 2.72 Å, and W−Ir = 2.80−2.86 Å), the B-LYP+ZORA/IV values are systematically too high, especially the W−W distance for which this technique yields 3.39 Å. Geometries obtained using only the local density approximation fare better, although even with LDA/II (which shows the best agreement overall with experiment for the tetrahedral geometry) there remains a tendency to overestimate the W−W distance. In examining the performance of the different levels of theory for the various neutral and doubly negatively charged stationary points on the C_{2v} $W_2Ir_2(CO)_{10}(\eta^5\text{-}C_5H_5)_2$ potential energy surface, it is apparent that LDA/II yields systematically shorter metal−metal bond lengths than LDA/IV (by between 0.02 and 0.07 Å), while B-LYP+ZORA/IV tends to give larger metal−metal separations than either implementation of LDA. The sole exception to this trend is for the butterfly dianion, for which B-LYP+ZORA/IV gives a somewhat diminished, albeit still nonbonded, W−W separation (4.79 Å), although even this is probably a consequence of the general tendency toward longer bonds with

(100) Levels of theory are denoted by the syntax (single-point calculation functional/basis set type)//geometry optimization functional/basis set type, where these functionals and basis set types are as described in the Theoretical Methods section.

B-LYP+ZORA: the Ir−Ir vector is markedly elongated in this structure (3.75 Å, cf. 3.28 Å at LDA/II), and contraction of W−W can be viewed as a geometric reaction to the Ir−Ir elongation. Overall, nonbonded metal−metal separations show a much larger dependence on level of theory than do bonding distances, and this result (that the more structurally rigid interactions are largely insensitive to level of theory) is a further factor supporting our use of the LDA/II geometries in subsequent single-point calculations.

The calculations show that the dianionic surface has a clear energetic preference for formation of a butterfly core structure lacking a W−W bond and possessing only a weak Ir−Ir interaction, in comparison with alternative tetrahedral core geometries with 10 or 9 carbonyl ligands. Note that, while the calculations suggest that it is the W−W and Ir−Ir bonds which are most sensitive to rupture, this is very probably a consequence of the imposition of C_{2v} symmetry (in the interests of computational expediency): it is much easier to cleave one W−W or Ir−Ir bond than to break all four W−Ir bonds simultaneously, but this symmetric constraint will obviously not apply in the real system. A more accurate perception of comparative bond strengths could be gained by performing further calculations in the absence of any symmetry constraints, but such calculations are computationally very demanding and we have not pursued this notion further at the present time. The removal of symmetry constraints would permit the sampling of alternative carbonyl ligand dispositions. However, the energetic differences between carbonyls adopting terminal or bridging coordination modes are known to be small compared to the energetic differences resultant upon core geometry variation;[101−103] it is therefore justifiable to maintain symmetry constraints in the interest of computational expediency. In contrast to the geometry change suggested by the calculations which results upon two-electron reduction, one-electron oxidation results in retention of the tetrahedral core geometry with some modification of metal−metal bond lengths (shortening of the heterometallic bonds, lengthening of the homometallic bonds).

We have identified a spin-allowed and symmetry-allowed transition, with an excitation energy of 8000 cm^{-1} according to the raw orbital energies obtained from the B-LYP+ZORA/IV//LDA/II calculation on the monocation. This transition, from the second-highest-occupied β-spin−orbital to the β-spin LUMO, is associated with orbitals which in each case show a preponderance of W (and less so, Ir) *d*-orbital character. Other possible transitions from β-spin−orbitals to the LUMO might feasibly be responsible for the observed feature, although in all these cases the agreement with the observed feature is at least 1600 cm^{-1} poorer. The low-energy transition in the UV−vis−NIR spectrum of **12** (Figure 8) is therefore likely to be largely σ-(W−W) → σ*(W−W) in character.

Discussion. The syntheses of the molybdenum−iridium clusters $MoIr_3(CO)_{11}(\eta^5\text{-}C_5H_{5-n}Me_n)$ [n = 1 (**5**), 4 (**6**), 5 (**7**)] and $Mo_2Ir_2(CO)_{10}(\eta^5\text{-}C_5H_{5-n}Me_n)_2$ [n = 1 (**8**), 4 (**9**), 5 (**10**)], which involve coordinating a range of methyl-substituted cyclopentadienyl groups of increasing bulk, have been shown to proceed similarly to those of the cyclopentadienyl-containing analogues $MoIr_3(CO)_{11}(\eta^5\text{-}C_5H_5)$ (**1**) and $Mo_2Ir_2(CO)_{10}(\eta^5\text{-}C_5H_5)_2$ (**3**), although in lower yields for **9** and **10**, probably a result of steric effects. The structural studies reveal core expansion on proceeding to the more sterically encumbered **7** and **10**, but the extent to which this reflects relief of steric strain is difficult to quantify; introduction of electron-releasing phosphine in proceeding to **13** also results in core expansion, and it is not possible to deconvolute electronic and steric contributions in the present system. Raman spectra of mixed-metal clusters may be a useful indication of average cluster core bond strength; for the present series, the frequency for the A_1 breathing mode correlates with the M−M′ bond lengths, the trends ν(Ir−Ir) > ν(Ir−M) > ν(M−M) and d(Ir−Ir) < d(Ir−M) < d(M−M) being observed. The $[MIr_3]$ and $[M_2Ir_2]$ clusters have accessible oxidation and reduction processes, the potentials for which correlate with expectations from systematic structural modification, suggesting that the electronic structure of this series can be controlled by appropriate change in cluster composition. The one-electron oxidation of the $[M_2Ir_2]$ clusters was examined by UV−vis−NIR and IR spectroelectrochemistry studies of **12**, and supported by approximate local density functional theory calculations. Proceeding from **12** to $\mathbf{12}^+$ involves retention of tetrahedral core geometry, but rearrangement to a selectively all-terminal carbonyl disposition. Oxidation also results in a low-energy band in the electronic spectrum assigned primarily to σ(M−M) → σ*(M−M), despite the presence of two different metals and three different bonds (M−M, M−Ir, Ir−Ir); this example of metal-specific redox processes in mixed-metal clusters complements previous demonstrations of metal-selective reactivity. This NIR transition is unprecedented in studies of clusters, to the best of our knowledge, but may have implications, for example, in switching of optical limiting, as clusters have been suggested as candidates for optical limiting applications.[104,105] The different reduction stoichiometry for the $[MoIr_3]$ and $[Mo_2Ir_2]$ clusters (one- and two-electron processes, respectively) suggests that the transferred electrons are possibly localized on the molybdenum atoms, perhaps concomitant with irreversible cleavage of the Mo−Mo bond. Calculations for the $[M_2Ir_2]^{2-}$ dianion support this suggestion, a butterfly geometry resulting from M−M cleavage being preferred. Calculations at various levels of theory have reiterated the caution one must apply in approaching a large system with heavy metal atoms, experimental geometries being reproduced only with inclusion of nonlocal and scalar relativistic corrections.

Experimental Section

General Conditions. Reactions were carried out under an atmosphere of argon or nitrogen using standard Schlenk techniques.[106] Glassware used in reactions involving sodium hydride was flame-dried under vacuum before use. All cluster complexes proved to be indefinitely stable in air as solids and for at least short periods of time in solution, and thus no precautions were taken to exclude air in their manipulation. Tetrahydrofuran was laboratory reagent (LR) grade. All other solvents used were analytical reagent (AR) grade. Unless stated otherwise, the following reaction solvents were dried and distilled under argon using standard methods: CH_2Cl_2 over CaH_2; THF over sodium

(101) Jang, J. H.; Lee, J. G.; Lee, H.; Xie, Y.; Schaefer, H. F., III. *J. Phys. Chem. A* **1998**, *102*, 5298.
(102) Hunstock, E.; Mealli, C.; Calhorda, M. J.; Reinhold, J. *Inorg. Chem.* **1999**, *38*, 5053.
(103) Hunstock, E.; Calhorda, M. J.; Hirva, P.; Pakkanen, T. A. *Organometallics* **2000**, *19*, 4624.
(104) Dagani, R. *Chem. Eng. News* **1996**, *January 1*, 24.
(105) Whittall, I. R.; McDonagh, A. M.; Humphrey, M. G.; Samoc, M. *Adv. Organomet. Chem.* **1999**, *43*, 349.
(106) Shriver, D. F.; Drezdzon, M. A. *The Manipulation of Air-sensitive Compounds*, 2nd ed.; Wiley: New York, 1986.

benzophenone ketyl. Acetic acid and CCl_4 were used without drying but were purged with nitrogen prior to use. Solvents used in the workup (including chromatography and crystallizations) were used as received. Petroleum spirit refers to a petroleum fraction of boiling range 60−80 °C. The cluster products were purified by thin-layer chromatography (TLC) on 20 × 20 cm^2 glass plates coated with Merck silica gel 60 PF_{254} (0.5 mm). Analytical TLC, used for monitoring the extent of reactions, was carried out on Merck aluminum sheets coated with 0.25 mm silica gel 60 PF_{254}.

Starting Materials and Reagents. The reagents tetramethylcyclopentadiene (mixture of isomers), pentamethylcyclopentadiene, sodium hydride (60% dispersion in oil), $Mo(CO)_6$, *n*-butyllithium solution (1.6 M in hexanes), PMe_3 (1 M in THF) (Aldrich), and granular zinc (Unilab), were purchased commercially and used as received. Methylcyclopentadiene was freshly distilled from methylcyclopentadiene dimer (Aldrich). The carbon monoxide used was high purity (Matheson), purchased from BOC gases. Literature procedures (or minor variations thereof) were used to synthesize $Mo(CO)_3(\eta^6$-xylene) (mixture of xylene isomers),[107] $IrCl(CO)_2$(*p*-toluidine),[108] $Ir_4(CO)_{12}$,[109] $WIr_3(CO)_{11}(\eta^5$-$C_5H_4Me)$,[90] and $W_2Ir_2(CO)_{10}(\eta^5$-$C_5H_4Me)_2$.[89] The *n*-butyllithium (nominally 1.6 M in hexanes) was titrated with diphenylacetic acid in THF prior to use to determine its exact concentration.[110]

Instruments. Infrared spectra were recorded on a Perkin-Elmer System 2000 FT-IR spectrometer in a solution cell with CaF_2 windows; spectral frequencies are recorded in cm^{-1}. All analytical spectra were recorded as solutions in either cyclohexane or CH_2Cl_2 (both AR grade). UV−vis spectra were recorded using a Cary 5G spectrophotometer as solutions in THF in 1 cm quartz cells, recorded over the range 240−1000 nm, and are reported in the form: λ_{max} (ϵ). ^{1}H NMR spectra were recorded in $CDCl_3$ (Cambridge Isotope Laboratories) using a Varian Gemini-300 spectrometer (at 300 MHz); spectra are referenced to residual $CHCl_3$ at 7.24 ppm. Secondary ion mass spectrometry (SIMS) spectra were recorded using a VG ZAB 2SEQ instrument (30 kV Cs^+ ions, current 1 mA, accelerating potential 8 kV, 3-nitrobenzyl alcohol matrix, solutions in CH_2Cl_2) at the Research School of Chemistry, Australian National University. All MS were calculated with the *m*/*z* based on ^{96}Mo, ^{183}W, and ^{192}Ir assignments, and are reported in the form: *m*/*z* (assignment, relative intensity). Elemental microanalyses were carried out by the Microanalysis Service Unit in the Research School of Chemistry, Australian National University. The Raman spectra were recorded using a Renishaw Ramascope 2000 with a HeNe (632.8 nm) laser, located at the Raman Imaging Microscopy Facility, University of Canberra, Australia.

Synthesis of $MoIr_3(CO)_{11}(\eta^5$-$C_5H_4Me)$ (5). Reaction of freshly distilled methylcyclopentadiene (0.50 mL, 5.0 mmol) with a THF solution of $Mo(CO)_3(\eta^6$-xylene) (600 mg, 2.10 mmol) at room temperature over 1 h gave the air-sensitive hydride $MoH(CO)_3(\eta^5$-C_5H_4-Me), a modification on a literature procedure.[84] The crude hydride may be used without purification in the cluster synthesis without decrease in yield, but purification may be effected (if desired) by sublimation at 60 °C at reduced pressure (ca. 0.1 mmHg). The $MoH(CO)_3(\eta^5$-C_5H_4-Me) prepared above was dissolved in CH_2Cl_2 (100 mL) and transferred to a 250 mL glass pressure bottle containing $IrCl(CO)_2$(*p*-toluidine) (118 mg, 0.302 mmol) and granular zinc (ca. 0.5 g). The bottle was first flushed with carbon monoxide, then pressurized to 40 psi and heated (with stirring) in an oil bath at 60 °C for 16 h. After being cooled to room temperature, the bottle was carefully vented and 2 mL of CCl_4 was added and the mixture stirred for 10 min. The orange solution was decanted or filtered into a flask, and the solution taken to dryness on a rotary evaporator. The residue was extracted into a small volume (ca. 3 mL) of CH_2Cl_2 and applied to preparative TLC plates. Elution with CH_2Cl_2/petroleum spirit (2/5) gave three bands:

The contents of the first band (R_f = 0.64) were extracted with CH_2Cl_2 and taken to dryness on a rotary evaporator to give a red powder identified as $Mo_2(CO)_6(\eta^5$-$C_5H_4Me)_2$ (52 mg).[111] IR (*c*-C_6H_{12}): ν(CO) 1957 vs, 1916 s, 1906 m cm^{-1}.

The contents of the second and major band (R_f = 0.47) were extracted with CH_2Cl_2 and recrystallized from CH_2Cl_2/methanol at 3 °C to afford orange crystals of $MoIr_3(CO)_{11}(\eta^5$-$C_5H_4Me)$ (**5**) (74 mg, 0.070 mmol, 69%). IR (*c*-C_6H_{12}): ν(CO) 2092 s, 2069 w, 2053 vs, 2046 vs, 2029 s, 2012 w, 1996 m, 1982 w, 1958 w, 1923 vw, 1870 w, 1819 vw, 1794 w cm^{-1}. UV−vis (THF): 271 sh (17.4), 318 sh (10.6), 353 sh (6.7), 492 sh (0.6) nm (10^3 L mol^{-1} cm^{-1}). ^{1}H NMR ($CDCl_3$): δ 5.05−5.00 (m, 4H, C_5H_4Me), 2.22 (s, 3H, C_5H_4*Me*). MS (SI): 1060 ([M]$^+$, 15), 1032 ([M − CO]$^+$, 30), 1004 ([M − 2CO]$^+$, 57), 976 ([M − 3CO]$^+$, 100), 948 ([M − 4CO]$^+$, 51), 920 ([M − 5CO]$^+$, 40), 892 ([M − 6CO]$^+$, 41), 864 ([M − 7CO]$^+$, 36), 836 ([M − 8CO]$^+$, 30). Anal. Calcd for $C_{17}H_7Ir_3MoO_{11}$ (1059.78): C, 19.27; H, 0.67. Found: C, 19.56; H, 0.54.

The contents of the third band (R_f = 0.25) were extracted with CH_2Cl_2 and taken to dryness on a rotary evaporator to give an orange powder identified as $MoCl(CO)_3(\eta^5$-$C_5H_4Me)$ (52 mg).[111] IR (*c*-C_6H_{12}): ν(CO) 2054 s, 1982 vs, 1959 s cm^{-1}.

Synthesis of $MoIr_3(CO)_{11}(\eta^5$-$C_5HMe_4)$ (6). Following the procedure described above for the synthesis of **5**, tetramethylcyclopentadiene (0.50 mL, 3.3 mmol) was reacted with a THF solution of $Mo(CO)_3(\eta^6$-xylene) (600 mg, 2.10 mmol) at room temperature over 1 h to give $MoH(CO)_3(\eta^5$-$C_5HMe_4)$. The crude hydride, $IrCl(CO)_2$(*p*-toluidine) (149 mg, 0.382 mmol), and granular zinc (ca. 0.5 g) were reacted at 60 °C under a 40 psi carbon monoxide atmosphere for 16 h. The cooled and vented solution was stirred with CCl_4, filtered, and taken to dryness, and the residue was extracted into CH_2Cl_2 and applied to preparative TLC plates. Elution with CH_2Cl_2/petroleum spirit (1/4) gave three bands:

The contents of the first band (R_f = 0.59, red), probably $Mo_2(CO)_6(\eta^5$-$C_5HMe_4)_2$, appeared to be in trace amounts and were not isolated.

The contents of the second and major band (R_f = 0.51) were extracted with CH_2Cl_2 and recrystallized from CH_2Cl_2/ethanol at 3 °C to afford orange crystals of $MoIr_3(CO)_{11}(\eta^5$-$C_5HMe_4)$ (**6**) (107 mg, 0.097 mmol, 76%). IR (*c*-C_6H_{12}): ν(CO) 2090 s, 2069 vw, 2057 s, 2049 vs, 2027 m, 2008 s, 1916 w, 1865 m, 1811 w, 1785 m cm^{-1}. UV−vis (THF): 267 sh (16.2), 317 sh (10.1), 370 sh (5.9), 474 sh (0.6) nm (10^3 L mol^{-1} cm^{-1}). ^{1}H NMR ($CDCl_3$): δ 4.23 (s, 1H, C_5HMe$_4$), 2.13, 1.92 (2 × s, 2 × 6H, C_5H*Me*$_4$). MS (SI): 1101 ([M]$^+$, 9), 1073 ([M − CO]$^+$, 17), 1045 ([M − 2CO]$^+$, 42), 1017 ([M − 3CO]$^+$, 100), 989 ([M − 4CO]$^+$, 31), 961 ([M − 5CO]$^+$, 43), 933 ([M − 6CO]$^+$, 35), 918 ([M − 6CO − Me]$^+$, 14), 905 ([M − 7CO]$^+$, 37), 890 ([M − 7CO − Me]$^+$, 16), 877 ([M − 8CO]$^+$, 26), 862 ([M − 8CO − Me]$^+$, 15), 849 ([M − 9CO]$^+$, 20), 834 ([M − 9CO − Me]$^+$, 15), 821 ([M − 10CO]$^+$, 10). Anal. Calcd for $C_{20}H_{13}Ir_3MoO_{11}$ (1101.86): C, 21.80; H, 1.19. Found: C, 21.87; H, 1.13.

The contents of the third band (R_f = 0.12) were extracted with CH_2Cl_2 and taken to dryness on a rotary evaporator to give an orange powder identified as $MoCl(CO)_3(\eta^5$-$C_5HMe_4)$ (58 mg). IR (*c*-C_6H_{12}): ν(CO) 2044 s, 1970 vs, 1946 s cm^{-1}. ^{1}H NMR ($CDCl_3$): δ 5.13 (s, 1H, C_5HMe$_4$), 1.93, 1.90 (2 × s, 2 × 6H, C_5H*Me*$_4$). MS (SI): 336 ([M]$^+$, 16), 308 ([M − CO]$^+$, 38), 301 ([M − Cl]$^+$, 47), 280 ([M − 2CO]$^+$, 43), 252 ([M − 3CO]$^+$, 100).

Synthesis of $MoIr_3(CO)_{11}(\eta^5$-$C_5Me_5)$ (7). Following the procedure described above for the synthesis of **5**, pentamethylcyclopentadiene (0.14 mL, 0.89 mmol) was reacted with a THF solution of $Mo(CO)_3(\eta^6$-xylene) (253 mg, 0.88 mmol) at room temperature over 2 h to give $MoH(CO)_3(\eta^5$-$C_5Me_5)$. The crude hydride, $IrCl(CO)_2$(*p*-toluidine) (74 mg, 0.189 mmol), and granular zinc (ca. 0.3 g) were reacted at 65 °C under a 40 psi carbon monoxide atmosphere for 16 h. The cooled and vented solution was stirred with CCl_4, filtered, and taken to dryness, and the residue was extracted into CH_2Cl_2 and applied to preparative TLC plates. Elution with CH_2Cl_2/petroleum spirit (2/7) gave three bands:

(107) Pidock, A.; Smith, J. D.; Taylor, B. W. *J. Chem. Soc. (A)* **1967**, 872.
(108) Klabunde, U. *Inorg. Synth.* **1974**, *15*, 82.
(109) Della Pergola, R.; Garlaschelli, L.; Martinengo, S. *Inorg. Synth.* **1990**, *28*, 245.
(110) Kofron, W. G.; Baclowski, L. M. *J. Org. Chem.* **1976**, *41*, 1879.
(111) Goldman, A. S.; Tyler, D. R. *Organometallics* **1984**, *3*, 449.

The contents of the first band ($R_f = 0.57$, red), probably $Mo_2(CO)_6(\eta^5\text{-}C_5Me_5)_2$, appeared to be in trace amounts and were not isolated.

The contents of the second and major band ($R_f = 0.35$) were extracted with CH_2Cl_2 and recrystallized from CH_2Cl_2/ethanol at 3 °C to afford orange crystals of $MoIr_3(CO)_{11}(\eta^5\text{-}C_5Me_5)$ (**7**) (51 mg, 0.046 mmol, 73%). A crystal grown by this method was selected for a single-crystal X-ray structural study. IR (c-C_6H_{12}): ν(CO) 2089 s, 2069 vw, 2056 s, 2049 vs, 2027 m, 2005 s, 1908 w, 1864 m, 1810 w, 1783 m cm^{-1}. ^{1}H NMR ($CDCl_3$): δ 1.92 (s, 15H, C_5Me_5). MS (SI): 1115 ([M]$^+$, 8), 1087 ([M − CO]$^+$, 9), 1059 ([M − 2CO]$^+$, 30), 1031 ([M − 3CO]$^+$, 100), 1003 ([M − 4CO]$^+$, 16), 975 ([M − 5CO]$^+$, 43), 947 ([M − 6CO]$^+$, 27), 932 ([M − 6CO − Me]$^+$, 7), 919 ([M − 7CO]$^+$, 44), 904 ([M − 7CO − Me]$^+$, 8), 891 ([M − 8CO]$^+$, 22), 876 ([M − 8CO − Me]$^+$, 8), 863 ([M − 9CO]$^+$, 16), 848 ([M − 9CO − Me]$^+$, 8), 835 ([M − 10CO]$^+$, 8), 820 ([M − 10CO − Me]$^+$, 5), 807 ([M − 11CO]$^+$, 4). Anal. Calcd for $C_{21}H_{15}Ir_3MoO_{11}$ (1115.88): C, 22.60; H, 1.35. Found: C, 22.36; H, 1.02.

The contents of the third band ($R_f = 0.13$) were extracted with CH_2Cl_2 and taken to dryness on a rotary evaporator to give an orange powder identified as $MoCl(CO)_3(\eta^5\text{-}C_5Me_5)$ (44 mg).[112] IR (c-C_6H_{12}): ν(CO) 2041 s, 1967 vs, 1940 s cm^{-1}.^{1}H NMR ($CDCl_3$): δ 1.91 (s, 15H, C_5Me_5).

Synthesis of $Mo_2Ir_2(CO)_{10}(\eta^5\text{-}C_5H_4Me)_2$ (8). Sodium hydride dispersion (257 mg, 6.43 mmol) was added to a solution of methylcyclopentadiene (0.75 mL, 7.5 mmol) in THF (50 mL) and the mixture was stirred at room temperature for 6 h (or until the sodium hydride is completely consumed and evolution of gas ceases). $Mo(CO)_6$ (1.00 g, 3.79 mmol) was added and the solution heated at reflux for 17 h. After the mixture was cooled to room temperature, the THF was removed in vacuo and replaced with CH_2Cl_2 (50 mL) (the Na[$Mo(CO)_3(\eta^5\text{-}C_5H_4Me)$] usually does not completely dissolve in the CH_2Cl_2). The pale pink suspension was stirred vigorously as $IrCl(CO)_2$(*p*-toluidine) (460 mg, 1.18 mmol) was added. The dark red-brown solution was stirred at room temperature for 30 min, before it was decanted away from any solid. The solid residue was rinsed with CH_2Cl_2, and the combined solutions were taken to dryness in vacuo. The brown residue was extracted into a small volume (ca. 3 mL) of CH_2Cl_2 and applied to preparative TLC plates. Elution with CH_2Cl_2/petroleum spirit (1/2) gave four bands:

The contents of the first band ($R_f = 0.69$, red), probably $Mo_2(CO)_6(\eta^5\text{-}C_5H_4Me)_2$, appeared to be in trace amounts and were not isolated.

The contents of the second band ($R_f = 0.62$) were extracted with CH_2Cl_2 and taken to dryness on a rotary evaporator to give an orange solid identified by solution IR as $MoIr_3(CO)_{11}(\eta^5\text{-}C_5H_4Me)$ (**5**) (ca. 1 mg).

The contents of the third and major band ($R_f = 0.44$) were extracted with CH_2Cl_2 and recrystallized from CH_2Cl_2/methanol at 3 °C to afford red-brown crystals of $Mo_2Ir_2(CO)_{10}(\eta^5\text{-}C_5H_4Me)_2$ (**8**) (485 mg, 0.478 mmol, 81%). IR (c-C_6H_{12}): ν(CO) 2061 m, 2054 m, 2031 vs, 2007 s, 1995 w, 1982 vs, 1958 m, 1933 m, 1884 w, 1863 m, 1811 w, 1764 m cm^{-1}; (CH_2Cl_2): ν(CO) 2060 s, 2031 vs, 2005 vs, 1986 sh, 1968 m, 1925 s, 1883 m, 1847 m, 1799 w, 1759m cm^{-1}. UV−vis (THF): 315 sh (12.7), 348 sh (9.7), 406 sh (5.0), 570 sh (1.2) nm (10^3 L mol^{-1} cm^{-1}). ^{1}H NMR ($CDCl_3$): δ 4.83 (m, 4H, C_5H_4Me), 4.79 (m, 4H, C_5H_4Me), 2.02 (s, 6H, C_5H_4Me). MS (SI): 1014 ([M]$^+$, 4), 986 ([M − CO]$^+$, 6), 958 ([M − 2CO]$^+$, 45), 930 ([M − 3CO]$^+$, 53), 902 ([M − 4CO]$^+$, 36), 874 ([M − 5CO]$^+$, 81), 846 ([M − 6CO]$^+$, 56), 818 ([M − 7CO]$^+$, 87), 803 ([M − 7CO − Me]$^+$, 28), 790 ([M − 8CO]$^+$, 66), 775 ([M − 8CO − Me]$^+$, 47), 762 ([M − 9CO]$^+$, 77), 747 ([M − 9CO − Me]$^+$, 88), 734 ([M − 10CO]$^+$, 34). Anal. Calcd for $C_{22}H_{14}Ir_2Mo_2O_{10}$ (1014.63): C, 26.04; H, 1.39. Found: C, 25.97; H, 1.17.

The contents of the fourth band ($R_f = 0.38$) were extracted with CH_2Cl_2 and taken to dryness on a rotary evaporator to give an orange powder identified by solution IR as $MoCl(CO)_3(\eta^5\text{-}C_5H_4Me)$ (88 mg).[111]

(112) Ginley, D. S.; Bock, C. R.; Wrighton, M. S. *Inorg. Chim. Acta* **1977**, *23*, 85.

Synthesis of $Mo_2Ir_2(CO)_{10}(\eta^5\text{-}C_5HMe_4)_2$ (9). A solution of *n*-butyllithium (1.50 mL, 1.31 M, 1.97 mmol) was added to tetramethylcyclopentadiene (0.3 mL, 1.98 mmol) in THF (20 mL) at −77 °C. A pale yellow suspension formed immediately, and the mixture was allowed to warm to room temperature over 18 h. $Mo(CO)_6$ (0.526 g, 1.99 mmol) was added and the solution heated at reflux for 20 h. After the mixture was cooled to room temperature, the THF was removed in vacuo and replaced with CH_2Cl_2 (50 mL). The pale pink suspension was stirred vigorously as $IrCl(CO)_2$(*p*-toluidine) (98 mg, 0.25 mmol) was added, and the dark red-brown solution was stirred at room temperature for 30 min. Acetic acid (0.5 mL) then CCl_4 (0.5 mL) were added and the mixture was stirred for a further 5 min before all volatile materials were removed in vacuo. The brown residue was extracted into a small volume (ca. 3 mL) of CH_2Cl_2 and applied to preparative TLC plates. Elution with CH_2Cl_2/petroleum spirit (1/2) gave three bands:

The contents of the first band ($R_f = 0.78$) were extracted with CH_2Cl_2 and taken to dryness on a rotary evaporator to give a red solid identified as $Mo_2(CO)_6(\eta^5\text{-}C_5HMe_4)_2$ (ca. 1 mg). IR (c-C_6H_{12}): ν(CO) 1970 m, 1941 vs, 1905 s cm^{-1}.

The contents of the second band ($R_f = 0.62$) were extracted with CH_2Cl_2 and taken to dryness on a rotary evaporator to give an orange solid identified by solution IR as $MoIr_3(CO)_{11}(\eta^5\text{-}C_5HMe_4)$ (**6**) (ca. 2 mg).

The contents of the third band ($R_f = 0.50$) were extracted with CH_2Cl_2 and recrystallized from CH_2Cl_2/ethanol at −18 °C to afford red-brown needle crystals of $Mo_2Ir_2(CO)_{10}(\eta^5\text{-}C_5HMe_4)_2$ (**9**) (84 mg, 0.076 mmol, 61%). IR (c-C_6H_{12}): ν(CO) 2057 s, 2027 vs, 2003 s, 1981 m, 1968 m, 1913 m, 1853 m, 1793 w, 1752 m cm^{-1}. UV−vis (THF): 320 sh (13.3), 351 sh (11.8), 408 sh (6.4), 548 sh (1.0) nm (10^3 L mol^{-1} cm^{-1}). ^{1}H NMR ($CDCl_3$): δ 5.28 (s, 1H, CH_2Cl_2), 4.53 (s, 2H, C_5HMe_4), 1.85, 1.83 (2 × s, 2 × 12H, C_5HMe_4). MS (SI): 1098 ([M]$^+$, 3), 1070 ([M − CO]$^+$, 5), 1042 ([M − 2CO]$^+$, 48), 1014 ([M − 3CO]$^+$, 46), 986 ([M − 4CO]$^+$, 27), 958 ([M − 5CO]$^+$, 83), 930 ([M − 6CO]$^+$, 34), 902 ([M − 7CO]$^+$, 76), 874 ([M − 8CO]$^+$, 100), 859 ([M − 8CO − Me]$^+$, 24), 846 ([M − 9CO]$^+$, 67), 831 ([M − 9CO − Me]$^+$, 38), 818 ([M − 10CO]$^+$, 52). Anal. Calcd for $C_{28}H_{26}Ir_2Mo_2O_{10}\cdot 0.5CH_2Cl_2$ (1098.79 + 52.47): C, 29.73; H, 2.36. Found: C, 29.92; H, 2.13.

The contents of the fourth band ($R_f = 0.32$) were extracted with CH_2Cl_2 and taken to dryness on a rotary evaporator to give an orange powder identified by solution IR as $MoCl(CO)_3(\eta^5\text{-}C_5HMe_4)$ (237 mg).

Synthesis of $Mo_2Ir_2(CO)_{10}(\eta^5\text{-}C_5Me_5)_2$ (10). Following the procedure described above for the synthesis of **9**, *n*-butyllithium (1.2 mL, 1.31 M, 1.57 mmol) was added to pentamethylcyclopentadiene (0.25 mL, 1.60 mmol) in THF (25 mL), $Mo(CO)_6$ (0.433 g, 1.64 mmol) was added, and the mixture was refluxed for 20 h. The THF was replaced with CH_2Cl_2 (40 mL), then $IrCl(CO)_2$(*p*-toluidine) (102 mg, 0.261 mmol) was added, and the dark red-brown solution was stirred at room temperature for 30 min. Acetic acid (0.5 mL) then CCl_4 (0.8 mL) were added and the mixture was stirred for a further 5 min before all volatile materials were removed in vacuo. The brown residue was extracted into a small volume of CH_2Cl_2 and applied to preparative TLC plates. Elution with CH_2Cl_2/petroleum spirit (1/2) gave four bands:

The contents of the first band ($R_f = 0.66$, red), probably $Mo_2(CO)_6(\eta^5\text{-}C_5Me_5)_2$, appeared to be in trace amounts and were not isolated.

The contents of the second band ($R_f = 0.59$) were extracted with CH_2Cl_2 and taken to dryness on a rotary evaporator to give an orange solid identified by solution IR as $MoIr_3(CO)_{11}(\eta^5\text{-}C_5Me_5)$ (**7**) (ca. 1 mg).

The contents of the third band ($R_f = 0.51$) were extracted with CH_2Cl_2 and recrystallized from CH_2Cl_2/methanol at 3 °C to afford orange crystals of $Mo_2Ir_2(CO)_{10}(\eta^5\text{-}C_5Me_5)_2$ (**10**) (52 mg, 0.046 mmol, 35%). A crystal grown by this method was selected for a single-crystal X-ray structural study. IR (c-C_6H_{12}): ν(CO) 2056 s, 2023 vs, 2000 s, 1978 m, 1958 m, 1914 m, 1850 m, 1797 w, 1744 m cm^{-1}. ^{1}H NMR ($CDCl_3$): δ 1.78 (s, C_5Me_5). MS (SI): 1126 ([M]$^+$, 8), 1098 ([M − CO]$^+$, 19), 1070 ([M − 2CO]$^+$, 100), 1042 ([M − 3CO]$^+$, 67), 1014

([M − 4CO]$^+$, 21), 986 ([M − 5CO]$^+$, 58), 958 ([M − 6CO]$^+$, 25), 930 ([M − 7CO]$^+$, 32), 902 ([M − 8CO]$^+$, 48), 887 ([M − 8CO − Me]$^+$, 13), 874 ([M − 9CO]$^+$, 36). Anal. Calcd for $C_{30}H_{30}Ir_2Mo_2O_{10}$ (1126.84): C, 31.98; H, 2.68. Found: C, 31.34; H, 2.34.

The contents of the fourth band (R_f = 0.42) were extracted with CH_2Cl_2 and taken to dryness on a rotary evaporator to give an orange powder identified by solution IR as $MoCl(CO)_3(\eta^5\text{-}C_5Me_5)$ (160 mg, 0.51 mmol).[112] IR (*c*-C_6H_{12}): ν(CO) 2041 s, 1967 vs, 1940 s cm^{-1}.

Reaction of $WIr_3(CO)_{11}(\eta^5\text{-}C_5H_4Me)$ (11) with PMe_3. An orange solution of $WIr_3(CO)_{11}(\eta^5\text{-}C_5H_4Me)$ (54.3 mg, 0.0473 mmol) and PMe_3 (70 μL, 1 M solution in THF, 0.070 mmol) in CH_2Cl_2 (15 mL) was stirred at room temperature for 17 h. The dark orange solution was taken to dryness in vacuo, then the residue was extracted into a small volume (ca. 2 mL) of CH_2Cl_2 and applied to preparative TLC plates. Elution with CH_2Cl_2/petroleum spirit (3/2) gave four bands:

The contents of the first band (R_f = 0.93) were extracted with CH_2Cl_2 and taken to dryness on a rotary evaporator to give an orange powder identified as unreacted $WIr_3(CO)_{11}(\eta^5\text{-}C_5H_4Me)$ (**11**) (13.3 mg, 0.0116 mmol).[90] IR (*c*-C_6H_{12}): ν(CO) 2091 m, 2053 s, 2046 vs, 2028 m, 1994 m, 1967 w cm^{-1}.

The contents of the second and major band (R_f = 0.71) were extracted with CH_2Cl_2 and recrystallized from CH_2Cl_2/methanol at 3 °C to afford orange crystals of $WIr_3(CO)_{10}(PMe_3)(\eta^5\text{-}C_5H_4Me)$ (**13**) (29.3 mg, 0.0245 mmol, 52%). A crystal grown by this method was selected for a single-crystal X-ray structural study. IR (*c*-C_6H_{12}): ν(CO) 2070 s, 2040 vs, 2031 w, 2022 m, 2013 s, 2004 m, 1992 vs, 1984 sh, 1956 w, 1916 m, 1839 m, 1825 m, 1799 m, 1746 m cm^{-1}. ^{1}H NMR ($CDCl_3$): δ 4.91 (br s, 2H, C_5H_4Me), 4.82 (m, 2H, C_5H_4Me), 2.35 (s, 3H, C_5H_4*Me*), 1.94 (d, J_{PH} = 11 Hz, 9H, P*Me*$_3$). ^{31}P NMR ($CDCl_3$): δ −30.3 (br s, *P*Me$_3$). MS (SI): 1194 ([M]$^+$, 17), 1166 ([M − CO]$^+$, 13), 1138 ([M − 2CO]$^+$, 50), 1110 ([M − 3CO]$^+$, 100), 1082 ([M − 4CO]$^+$, 42), 1054 ([M − 5CO]$^+$, 11), 1024 ([M − 6CO − 2H]$^+$, 25), 996 ([M − 7CO − 2H]$^+$, 18), 968 ([M − 8CO − 2H]$^+$, 8), 956 ([M − 8CO − CH_2]$^+$, 5), 940 ([M − 9CO − 2H]$^+$, 6), 928 ([M − 9CO − CH_2]$^+$, 7), 912 ([M − 10CO − 2H]$^+$, 6). Anal. Calcd for $C_{19}H_{16}Ir_3O_{10}PW$ (1195.76): C, 19.08; H, 1.35. Found: C, 19.02; H, 1.30.

The contents of the third band (R_f = 0.61) were extracted with CH_2Cl_2 and taken to dryness on a rotary evaporator to give an orange powder identified as $WIr_3(CO)_9(PMe_3)_2(\eta^5\text{-}C_5H_4Me)$ (**14**) (17.0 mg, 0.0137 mmol, 29%). IR (*c*-C_6H_{12}): ν(CO) 2044 s, 2027 w, 2005 s, 1994 sh, 1987 vs, 1977 s, 1964 m, 1954 m, 1897 m, 1807 m, 1759 m, 1733 s cm^{-1}. ^{1}H NMR ($CDCl_3$): δ 4.93 (m, 2H, C_5H_4Me), 4.74 (br s, 2H, C_5H_4Me), 2.42 (s, 3H, C_5H_4*Me*), 1.97 (d, J_{PH} = 10 Hz, 18H, P*Me*$_3$). ^{31}P NMR ($CDCl_3$): no distinct resonances. MS (SI): 1214 ([M − CO]$^+$, 8), 1186 ([M − 2CO]$^+$, 26), 1158 ([M − 3CO]$^+$, 100), 1130 ([M − 4CO]$^+$, 39), 1102 ([M − 5CO]$^+$, 13), 1072 ([M − 6CO − 2H]$^+$, 44), 1058 ([M − 6CO − CH_4]$^+$, 8), 1042 ([M − 6CO − 2CH_4]$^+$, 18), 1030 ([M − 7CO − CH_4]$^+$, 10), 1014 ([M − 7CO − 2CH_4]$^+$, 9), 998 ([M − 6CO − PMe_3]$^+$, 13), 986 ([M − 8CO − 2CH_4]$^+$, 9), 970 ([M − 7CO − PMe_3]$^+$, 12), 958 ([M − 9CO − 2CH_4]$^+$, 12), 942 ([M − 8CO − PMe_3]$^+$, 10).

The contents of the fourth band (R_f = 0.25) contained a trace amount of an unidentified solid.

Reaction of $W_2Ir_2(CO)_{10}(\eta^5\text{-}C_5H_4Me)_2$ (12) with PMe_3. A red-brown solution of $W_2Ir_2(CO)_{10}(\eta^5\text{-}C_5H_4Me)_2$ (53.9 mg, 0.0453 mmol) and PMe_3 (45 μL, 1 M solution in THF, 0.045 mmol) in CH_2Cl_2 (15 mL) was stirred at room temperature for 18 h. The solution was taken to dryness in vacuo, then the residue was extracted into a small volume (ca. 2 mL) of CH_2Cl_2 and applied to preparative TLC plates. Elution with CH_2Cl_2/petroleum spirit (3/2) gave three bands:

The contents of the first band (R_f = 0.79) were extracted with CH_2Cl_2 and taken to dryness on a rotary evaporator to give a red-brown powder identified as unreacted $W_2Ir_2(CO)_{10}(\eta^5\text{-}C_5H_4Me)_2$ (**12**) (10.1 mg, 0.0085 mmol).[89] IR (*c*-C_6H_{12}): ν(CO) 2063 m, 2028 s, 2006 m, 1995 m, 1982 m, 1965 w, 1948 w, 1921 w, 1890 w, 1827 w cm^{-1}.

The contents of the second and major band (R_f = 0.50) were extracted with CH_2Cl_2 and recrystallized from CH_2Cl_2/methanol at 3 °C to afford red-brown crystals of $W_2Ir_2(CO)_9(PMe_3)(\eta^5\text{-}C_5H_4Me)_2$ (**15**) (34.5 mg, 0.0278 mmol, 61%). IR (*c*-C_6H_{12}): ν(CO) 2024 s, 1999 m, 1984 vs, 1970 s, 1953 m, 1915 w, 1890 m, 1864 m, 1831 m, 1767 w, 1739 m cm^{-1}. ^{1}H NMR ($CDCl_3$): δ 4.84 (m, 4H, C_5H_4Me), 4.62 (m, 4H, C_5H_4-Me), 2.16 (s, 6H, C_5H_4*Me*), 1.89 (d, J_{PH} = 11 Hz, 9H, P*Me*$_3$). ^{31}P NMR ($CDCl_3$): no distinct resonances. MS (SI): 1208 ([M − CO]$^+$, 8), 1180 ([M − 2CO]$^+$, 28), 1152 ([M − 3CO]$^+$, 65), 1124 ([M − 4CO]$^+$, 57), 1096 ([M − 5CO]$^+$, 100), 1068 ([M − 6CO]$^+$, 42), 1038 ([M − 7CO − 2H]$^+$, 41), 1010 ([M − 8CO − 2H]$^+$, 31), 992 ([M − 6CO − PMe_3]$^+$, 26), 980 ([M − 8CO − 2CH_4]$^+$, 40), 964 ([M − 7CO − PMe_3]$^+$, 44), 952 ([M − 9CO − 2CH_4]$^+$, 19). Anal. Calcd for $C_{24}H_{23}Ir_2O_9PW_2$ (1238.52): C, 23.27; H, 1.87. Found: C, 23.83; H, 2.10.

The contents of the third band (R_f = 0.21) were extracted with CH_2Cl_2 and taken to dryness on a rotary evaporator to give a brown powder identified as $W_2Ir_2(CO)_8(PMe_3)_2(\eta^5\text{-}C_5H_4Me)_2$ (**16**) (ca. 1 mg). This product was found to have limited stability, decomposing slowly over days. IR (CH_2Cl_2): ν(CO) 1978 sh, 1956 vs, 1925 s, 1862 m, 1824 sh, 1789 m, 1708 s cm^{-1}. ^{1}H NMR ($CDCl_3$): δ 4.61 (m, 8H, C_5H_4Me), 2.16 (s, 6H, C_5H_4*Me*), 1.81 (d, J_{PH} = 10 Hz, 18H, P*Me*$_3$).

Electrochemical Studies. The cyclic voltammograms were recorded using a MacLab 400 interface and MacLab potentiostat from ADInstruments. The supporting electrolyte was 0.25 M $(NBu^n_4)PF_6$ in distilled, deoxygenated CH_2Cl_2. Solutions containing ca. 2 × 10^{-3} mol L^{-1} complex were maintained under argon. Measurements were carried out using a platinum disk working (1 mm diameter), platinum auxiliary, and Ag/AgCl reference electrodes, using the ferrocene/ferrocenium redox couple as an internal reference (0.56 V). The controlled potential coulometry experiments were carried out using a PAR 273A potentiostat connected to platinum gauze working and auxiliary electrodes, and Ag/AgCl reference electrode in a two compartment (5 mL) electrolytic cell. The UV−vis spectroelectrochemical spectra were recorded on a Cary 5E spectrophotometer over the range 4000−45000 cm^{-1} (2500−222 nm). Solution spectra of the oxidized species at 233 K were obtained by electrogeneration (Thompson 401E potentiostat) at a Pt gauze working electrode within a cryostatted optically transparent thin-layer electrochemical (OTTLE) cell, path length 0.5 mm, mounted within the spectrophotometer.[113] The IR spectroelectrochemical spectrum was recorded on a Perkin-Elmer System 2000 spectrometer over the range 600−8000 cm^{-1} using a mid-IR TGS detector. Solution spectra of the oxidized species at ca. 233 K were obtained by electrogeneration (PAR 170 potentiostat) at a cryostatted Pt disk working electrode (10 mm diameter) that also acted as a mirror within a 5 mL infrared reflection−absorption spectroscopic (IRRAS) cell.[114] A NaCl cell window was used and the solution beam path length was ca. 0.5 mm. The cell was mounted within the spectrometer on a Specac attachment containing beam-steering optics, and the sample and detector compartments were purged with dry nitrogen gas over the course of the experiment to avoid fogging of the optics.

X-ray Crystallographic Studies. Crystals suitable for X-ray structural studies were grown by liquid diffusion techniques, as described above. A single crystal was glued to a glass fiber and mounted on either a Rigaku AFC6S diffractometer (**7**, **10**) or Nonius KappaCCD diffractometer (**13**) located at the Research School of Chemistry, Australian National University. The data collection and structural refinement details for compounds **7**, **10**, and **13** are summarized in Table 4. All aspects of the solution and refinement were handled within the teXsan software package.[115] The structures were solved by direct (**7**, **10**)[116] or Patterson (**13**)[117] methods, and expanded using difference

(113) Duff, C. M.; Heath, G. A. *Inorg. Chem.* **1991**, *30*, 2528.
(114) Best, S. P.; Clark, R. J. H.; McQueen, R. C. S.; Cooney, R. P. *Rev. Sci. Instrum.* **1987**, *58*, 2071.
(115) *teXsan: Single-Crystal Structure Analysis Software*, Version 1.8; Molecular Structure Corporation: The Woodlands, TX 77381, 1997.
(116) Altomare, A.; Cascarano, M.; Giacovazzo, C.; Guagliardi, A.; Burla, M. C.; Polidori, G.; Camalli, M. *J. Appl. Crystallogr.* **1994**, *27*, 425.

Fouriertechniques.[118] Non-hydrogen atoms were refined anisotropically; hydrogen atoms were included in idealized positions which were frequently recalculated. The final cycle of full-matrix least-squares refinement on F was based on N_{obs} reflections ($I > 2\sigma(I)$) and converged to R and R_w.

Theoretical Methods. Approximate density functional theory calculations were performed on Linux-based Pentium III 600 MHz computers using the Amsterdam Density Functional (ADF) program, version ADF 2000.01,[119] developed by Baerends et al.[120−125] Calculations on $W_2Ir_2(CO)_{10}(\eta^5\text{-}C_5H_5)_2$ structures, in various charge states, were performed in C_{2v} symmetry, with the implicit assumption that the two cyclopentadienyl rings were superimposable on each other by reflection in a mirror plane (which contained the Ir−Ir axis and which was perpendicular to the W−W axis). All carbonyls were initially assumed to be terminally coordinated, but bridging interactions were permitted within the imposed symmetry constraints. Electrons in orbitals up to and including 1*s* {C, O} and 4*f* (but excluding 5*s* and 5*p*) {W, Ir} were treated in accordance with the frozen-core approximation. Geometry optimizations on structures containing a quasitetrahedral W_2Ir_2 core (all W and Ir atoms bonded to each other) were attempted for the 2^+, 1^+, 0, 1^-, and 2^- charge states, using the local density approximation (LDA) to the exchange potential,[126,127] and the correlation potential of Vosko, Wilk, and Nusair,[128] with a double-ζ quality Slater-type orbital (Type II) basis set for each atom. Calculations were spin-restricted unless considerations of electronic configuration (i.e., a spin-doublet or spin-triplet electronic state) dictated an unrestricted calculation.

Nonlocal and relativistic corrections to the local density approximation were effected through single-point calculations on the LDA/Type II optimized geometries, employing the B-LYP nonlocal exchange and correlation functionals and the ZORA scalar relativistic correction[129] in conjunction with triple-ζ (Type IV) basis sets for each atom. To test the reliability of the LDA/Type II optimized geometries, some additional optimizations were performed (for the spin-restricted examples among the range of $W_2Ir_2(CO)_{10}(\eta^5\text{-}C_5H_5)_2^{n\pm}$ structures) using the Type IV basis set, either with LDA and the VWN local correlation functional, or with the B-LYP and ZORA corrections. In all of these results it was apparent that the relative energies obtained merely by application of the local density approximation were very different from those obtained after correction for relativistic effects: nevertheless, changes in optimized geometry between the LDA/Type II and LDA/Type IV optimizations were only minor, suggesting that basis set truncation in the smaller Type II basis is not a significant source of error. Likewise, the relative energies of different structures obtained after implementation of the B-LYP and ZORA corrections were essentially unaffected by the method of geometry optimization (i.e., whether optimization was performed at the LDA/Type II or at the more rigorous B-LYP+ZORA/Type IV level of theory). We concluded, from this analysis, that the LDA/Type II optimizations are sufficiently reliable that they can satisfactorily be used in subsequent single-point calculations, and followed this strategy in determining relative energies of different structures and/or different charge states, the results from which are tabulated in Table 7.

Acknowledgment. We thank the Australian Research Council (ARC) for financial support in the form of Large Grants (M.G.H., R.S.) and the funds to purchase the KappaCCD diffractometer, and Johnson-Matthey Technology Centre for the generous loan of iridium salts (M.G.H.). We thank Dr. D. C. R. Hockless for collection of X-ray diffraction data (compounds **7** and **10**). M.G.H. holds an ARC Australian Senior Research Fellowship, N.T.L. was an Australian Postgraduate Awardee, and J.P.B. thanks the Australian-American Fulbright Commission for a Senior Scholar Award.

Supporting Information Available: Crystallographic files (CIF). This material is available free of charge via the Internet at http://pubs.acs.org.

JA0173829

(117) Beurskens, P. T.; Admiraal, G.; Beurskens, G.; Bosman, W. P.; Garcia-Granda, S.; Gould, R. O.; Smits, J. M. M.; Smykalla, C. *PATTY*: *The DIRDIF program system*. Technical Report of the Crystallography Laboratory; University of Nijmegen: Nijmegen, The Netherlands, 1992.
(118) Beurskens, P. T.; Admiraal, G.; Beurskens, G.; Bosman, W. P.; de Gelder, R.; Israel, R.; Smits, J. M. M. *The DIRDIF-94 Program System*. Technical Report of the Crystallography Laboratory; University of Nijmegen: Nijmegen, The Netherlands, 1994.
(119) Baerends, E. J.; Bérces, A.; Bo, C.; Boerrigter, P. M.; Cavallo, L.; Deng, L.; Dickson, R. M.; Ellis, D. E.; Fan, L.; Fischer, T. H.; Fonseca Guerra, C.; van Gisbergen, S. J. A.; Groeneveld, J. A.; Gritsenko, O. V.; Harris, F. E.; van den Hoek, P.; Jacobsen, H.; van Kessel, G.; Kootstra, F.; van Lenthe, E.; Osinga, V. P.; Philipsen, P. H. T.; Post, D.; Pye, C.; Ravenek, W.; Ros, P.; Schipper, P. R. T.; Schreckenbach, G.; Snijders, J. G.; Sola, M.; Swerhone, D.; te Velde, G.; Vernooijs, P.; Versluis, L.; Visser, O.; van Wezenbeek, E.; Wiesenekker, G.; Wolff, S. K.; Woo, T. K.; Ziegler, T. *ADF*, *2000.01*, 2000.
(120) Baerends, E. J.; Ellis, D. E.; Ros, P. *Chem. Phys.* **1973**, *2*, 42.
(121) Baerends, E. J.; Ros, P. *Chem. Phys.* **1973**, *2*, 52.
(122) Baerends, E. J.; Ros, P. *Int. J. Quantum Chem.* **1978**, *s12*, 169.
(123) Versluis, L.; Ziegler, T. J. *J. Chem. Phys.* **1988**, *88*, 322.
(124) te Velde, G.; Baerends, E. J. *J. Comput. Chem.* **1992**, *99*, 84.
(125) Fonseca Guerra, C.; Snijders, J. G.; te Velde, G.; Baerends, E. J. *Theor. Chem. Acc.* **1998**, *99*, 391.
(126) Parr, R. G.; Yang, W. *Density Functional Theory of Atoms and Molecules*; Oxford University Press: New York, 1989.
(127) Ziegler, T. *Chem. Rev.* **1991**, *91*, 1.
(128) Vosko, S. H.; Wilk, L.; Nusair, M. *Can. J. Phys.* **1980**, *58*, 1200.
(129) van Lenthe, E.; Baerends, E. J.; Snijders, J. G. J. *Chem. Phys.* **1993**, *99*, 4597.